Chapter 4

A New UVX Catalogue for the 2-degree Field QSO Survey

4.1 Introduction - the need for a new QSO survey

As discussed in Chapter 1, QSOs are fundamental probes of the Universe at high redshift. Clustering statistics of present surveys (Chapter 3) are beginning to answer important cosmological questions. The ability to measure clustering at different epochs allows us to make estimates of the density parameter Ω_0, while geometric tests can be used to measure Λ, both of these parameters being fundamental to cosmology. Chapter 3 clearly showed that significantly larger QSOs surveys are required to obtain certain measurements of these parameters, in particular, a survey with a high number density of QSOs. It is the production of a large, deep, wide-field QSO survey that we turn to in this chapter.

The past decade has seen a vast increase in the number of known QSOs. These have been found using a variety of optical and non-optical selection methods. Optical selection methods can be divided into three areas, the first being selection based on low dispersion spectra obtained from objective prism plate surveys. This process allows a measure of the shape of the QSO candidate continuum, effectively an estimate of the colour, as well as the identification of broad emission lines, the latter being particularly useful for identifying high redshift, $z > 2$, QSOs in which the continuum is becoming redder. The advantages of this method include well defined selection for a given flux and spectral type and low levels of contamination by galactic stars. There are two main disadvantages; the first is that objective prism spectra from nearby objects will overlap, making the measurement of the continuum or lines difficult or impossible. The second disadvantage is that present objective prism surveys cannot expect to reach magnitudes fainter than $b_J \sim 19 - 20$, due to both the large relative sky flux in such observations and the increase in number density leading to overlapping spectra. However this method remains the most effective for detection of bright QSOs in samples such as the Hamburg/ESO survey

(Wisotzki et al., 1996) covering the magnitude range $13 \leq B \leq 17.5$, and the LBQS (Hewett et al., 1995) over the range $16 \leq b_J \leq 18.5$.

Alternatively the selection process can be based solely on broad band colours. The first method of this type to be employed was the ultra-violet excess (UVX) technique (Schmidt & Green, 1983; Shanks et al., 1983b), which uses the extremely blue colour ($U - B < -0.3$) of QSOs to differentiate them from ordinary galactic stars. This has been applied in the Homogeneous Bright QSO Survey (Cristiani et al., 1995) to a depth of $B \simeq 18.75$, the Durham/AAT QSO survey (Boyle et al., 1990) to a depth of $B \simeq 21$, as well as many other samples. UVX selection has the advantage of being able to reach fainter magnitudes, although with a higher fraction of contaminating stars than in the objective prism method. For example, the Durham/AAT QSO sample contains a total of 420 QSOs along with 57 narrow emission line galaxies, spectroscopy of the candidates also found 824 galactic stars (including a number of white dwarfs), the best possible photometric accuracy is required to reduce this level of contamination. As well as the relatively high rate of contamination there are several selection effects to consider when using the UVX technique. As objects are only selected if they have a stellar point spread function (PSF), QSOs at low redshift can be rejected if their host galaxy is sufficiently bright to create a non-stellar PSF. At redshifts higher than $z = 2.2$ the Lyα emission line moves into the B band so that the QSOs generally have redder $U - B$ colours. The UVX selection can therefore only be complete below this redshift. Within these constraints the UVX selection technique is consistent in selecting the vast majority ($> 95\%$) of QSOs detected via other selection methods. To reach higher redshifts multi-colour selection procedures are used, such as $B - R$ vs. $U - B$ (Shanks et al., 1983a; Warren et al., 1987; Boyle et al., 1991). Multi-colour photometry also further reduces stellar contamination, as an increase in the number of bands observed allows tighter constraints to be placed on the spectral energy distribution (SED) of the QSOs. A detailed discussion of multi-colour QSO selection is given by Warren et al., (1991).

A third optical selection process is based on QSO variability. QSO luminosities are known to vary over a large range of time scales. By using the long baseline provided by photographic plate archives it is possible to detect these variations (Koo et al., 1986; Veron & Hawkins, 1995). Problems with this method lie in the luminosity dependence of the variability (Cristiani et al., 1996) and the uncertain completeness, with surveys based on variability generally producing lower number densities of QSOs than the UVX selection method. QSO variability will also have an effect on colour selection methods, which we will discuss further in Section 4.3.

The very first QSOs discovered were found on the basis of their strong radio flux (Schmidt, 1963). However it was soon apparent that the majority of QSOs ($> 90\%$) did not show this radio emission but were radio-quiet. New deep radio surveys such as the FIRST Bright QSO survey (Gregg et al., 1996) reach to deeper flux levels and are starting to find *radio-quiet* objects. 50% of the QSOs in the FIRST sample are radio-quiet (as opposed to radio silent), that is $L_{21\mathrm{cm}} < 10^{32.5}\mathrm{ergs}^{-1}$. All-sky X-ray surveys have also produced significant numbers of QSOs, these include the Einstein

Extended Medium Sensitivity Survey (EMSS) (Stocke et al., 1991) and the ROSAT All-Sky Survey (Bade et al., 1995). There are also a number of deeper ROSAT pointings in particular regions of the sky (Shanks et al., 1991; Boyle et al., 1993).

This combination of selection techniques has provided a total of $\sim$ 9000 QSOs (Veron-Cetty & Veron, 1996), a collection of QSOs which is, of course, completely inhomogeneous, and as such cannot be used as a whole for a range of statistical tests. To carry out tests on clustering in particular it is imperative to start with a homogeneous sample. Clustering studies are also highly dependent on the space density of QSOs. It was noted in Chapter 3 that the LBQS was not an ideal sample with which to study clustering, the surface density of QSOs in this sample being a factor of $\sim$ 20 lower than in the Durham/AAT QSO survey. It is therefore imperative that the depth of any QSO survey to be used for clustering analysis reaches at least the magnitude of the turnover in the number-magnitude relation for QSOs, (Eqs. 3.1 and 3.2), at $B \sim 19.5^m$. A large contiguous area is also important for measurements of large-scale structure, allowing the complete sampling of a large volume, and the matching of photometry across the catalogue.

The new 2-degree Field (2dF) instrument on the Anglo-Australian telescope is a multi-object fibre-fed spectrograph, which can obtain spectra for $\sim$ 400 objects at a time over a field of view fully 2 degrees in diameter. This huge multiplexing gain opens the door to a new generation of redshift surveys an order of magnitude larger in size than previously possible. To take advantage of this instrument a large wide-field catalogue of QSO candidates was needed. Not only this, but to obtain maximum scientific gain from the survey, this catalogue should be uniform, complete and photometrically accurate. To obtain a sufficient number density of QSOs a colour selection process was required, and the only method available to cover sufficient area was the use of photographic plates. The UVX selection method was an obvious choice, being proven to select the overwhelming majority of QSOs at redshifts $z < 2.2$.

Below we describe the construction of the 2dF QSO survey input catalogue, in particular the southern strip at $\delta = -30°$. A similar northern strip was constructed by Robert Smith (IoA, Cambridge) using the same process. We paid particular attention to the correction for plate field effects and obtaining accurate and reliable CCD photometric sequences with which to calibrate and linearize our photographic magnitudes. We have also estimated the level of completeness we expect from the distribution of all the known QSOs which lie in our survey region. We will discuss several factors which may contribute to incompleteness.

Table 4.1: Details of the UKST III-aJ survey plates used in the Southern 2dF QSO survey.

UKST field	Plate No.	R.A.(B1950)	Dec. (B1950)	Date
f466	J5113c	21 51 00	-30 00 00	25/06/79
f467	J3514cc	22 14 00	-30 00 00	18/08/77
f468	J6436	22 37 00	-30 00 00	30/09/80
f469	J3508	23 00 00	-30 00 00	17/08/77
f470	J3525c	23 23 00	-30 00 00	18/08/77
f471	J6138	23 46 00	-30 00 00	17/07/80
f409	J2693c	00 00 00	-30 00 00	17/11/76
f410	J2696c	00 23 00	-30 00 00	18/11/76
f411	J4606c	00 46 00	-30 00 00	25/10/78
f412	J3516c	01 09 00	-30 00 00	18/08/77
f413	J3774c	01 32 00	-30 00 00	03/12/77
f414	J3579c	01 55 00	-30 00 00	15/09/77
f415	J4607c	02 18 00	-30 00 00	25/10/78
f416	J4608c	02 41 00	-30 00 00	25/10/78
f417	J3818c	03 04 00	-30 00 00	12/12/77

4.2 Producing a Homogeneous UVX Catalogue

For the reasons discussed above we wish to produce a deep, uniform UVX catalogue to use as a candidate list for the 2dF QSO survey. The selection procedure is based on scans of $6° \times 6°$ United Kingdom Schmidt Telescope (UKST) III-aJ and U plates scanned by the Automatic Plate Measurement (APM) facility at the Royal Greenwich Observatory (RGO), Cambridge. Table 4.1 gives details of the UKST III-aJ plates used. These are part of the 1st Epoch UKST Sky Survey and use the III-aJ emulsion in conjunction with a Schott GG395 filter to produce the blue photographic passband which we will denote as $b_{\rm J}$. The conversion between this band and the standard Johnson-Kron-Cousins photometric system is given by

$$b_{\rm J} = B - 0.28(B - V) \tag{4.1}$$

(Blair & Gilmore, 1982) where B and V denote the standard passbands. The U plates have mostly been obtained over a period of ~ 5 years, in preparation for this survey. A large number of these exposures have been taken on film, rather than glass plate. In both cases the UG1 filter was used, in conjunction with the III-aJ or 4415 emulsion for plates or films respectively. Blair & Gilmore also measure the colour transform from the standard photo-electric system to photographic u, finding

$$u = U - 0.03(U - B) \tag{4.2}$$

where u is the photographic system, although here this is defined by the IIa-O emulsion and the UG1 filter. The error on the colour term in this case is ± 0.05, so given that the colour term is not significant we shall define our photographic u-band magnitudes as $u = U$, where U is the standard photo-electric magnitude. Table 4.2 gives details of the u plates. Multiple plates were obtained in each survey area in order to, (i) ensure at least one good quality plate reaches the depth of the survey and (ii) allow us to use co-addition of the image intensities, in order to reduce the intrinsic r.m.s. scatter of the magnitudes at faint limits. As can be seen from Table 4.2 the depth of the plates is varied, from $u = 19.4$ in the very worst case to $u = 21.6$ for the best two plates. A small number of plates (four in all) were not scanned, due to trailing and other plate defects.

Table 4.2: Details of the UKST u plates used in the Southern 2dF QSO survey. Exposures labelled (f) are films, those marked * are poor quality and were not scanned

UKST Field	Plate No.	R.A.(B1950)	Dec. (B1950)	Date	Exposure time	Plate limit
f466	U15162(f)	21 51 00	-30 00 00	17/09/92	1800	20.7
	U15167(f)	21 51 00	-30 00 00	18/09/92	1800	20.3
	U15222(f)	21 51 00	-30 00 00	20/10/92	1800	20.4
	U15226	21 51 00	-30 00 00	21/10/92	1800	21.5
f467	U15706	22 14 00	-30 00 00	18/08/93	1800	21.2
	U15718(f)	22 14 00	-30 00 00	20/08/93	1800	21.4
f468	U15169(f)	22 37 00	-30 00 00	20/09/92	1800	20.8
	U15170	22 37 00	-30 00 00	20/09/92	1800	20.9
	U15750	22 37 00	-30 00 00	07/09/93	1800	21.4
	U16781*	22 37 00	-30 00 00	20/09/95	900	-
	U16840(f)	22 37 00	-30 00 00	23/10/95	1000	21.2
f469	U15231	23 00 00	-30 00 00	22/10/92	1800	21.6
	U15235(f)	23 00 00	-30 00 00	01/11/92	1225	19.8
	U15642(f)	23 00 00	-30 00 00	26/07/93	1800	21.2
f470	U1776	23 23 00	-30 00 00	14/08/75	900	20.1
	U15654(f)	23 23 00	-30 00 00	28/07/93	1800	19.4
	U15724	23 23 00	-30 00 00	21/08/93	1800	21.6
	U16730(f)*	23 23 00	-30 00 00	21/08/95	670	-
	U16838(f)	23 23 00	-30 00 00	22/10/95	900	19.8
	U16843(f)	23 23 00	-30 00 00	27/10/27	900	20.9
f471	U15733	23 46 00	-30 00 00	22/08/93	1800	21.4
	U15738(f)	23 46 00	-30 00 00	23/08/93	1800	21.0
f409	U1833	00 00 00	-30 00 00	04/10/75	900	19.8
	U16247(f)	00 00 00	-30 00 00	14/08/94	900	20.4
	U16812(f)	00 00 00	-30 00 00	14/10/95	900	20.8
f410	U16743(f)	00 23 00	-30 00 00	25/08/95	900	20.5
	U16813(f)	00 23 00	-30 00 00	14/10/95	900	20.8
	U17246(f)	00 23 00	-30 00 00	13/09/96	900	20.6
f411	U14503	00 46 00	-30 00 00	01/09/91	1800	20.3
	U15202(f)	00 46 00	-30 00 00	01/10/92	900	20.6
	U15223(f)	00 46 00	-30 00 00	20/10/92	900	20.5
	U15227(f)	00 46 00	-30 00 00	21/10/92	900	20.7

Table 4.2: u plates: continued

UKST Field	Plate No.	R.A.(B1950)	Dec. (B1950)	Date	Exposure time	Plate limit
	U15719(f)	00 46 00	-30 00 00	20/08/93	900	21.0
f412	U13970	01 09 00	-30 00 00	06/11/90	1800	19.3
	U16335(f)	01 09 00	-30 00 00	03/10/94	900	21.0
	U16340(f)	01 09 00	-30 00 00	05/10/94	900	21.3
	U16389(f)	01 09 00	-30 00 00	08/11/94	900	21.3
f413	U16751(f)	01 32 00	-30 00 00	17/08/95	900	20.5
	U16814(f)	01 32 00	-30 00 00	14/10/95	900	19.8
	U17263(f)	01 32 00	-30 00 00	15/09/96	900	20.9
f414	U16751(f)	01 55 00	-30 00 00	27/08/95	900	20.6
	U16782(f)	01 55 00	-30 00 00	21/09/95	900	20.6
	U16824(f)	01 55 00	-30 00 00	16/10/95	900	21.1
f415	U16427(f)	02 18 00	-30 00 00	02/12/94	900	20.9
	U16744(f)	02 18 00	-30 00 00	25/08/95	900	20.9
f416	U2830*	02 41 00	-30 00 00	19/01/77	900	-
	U7348	02 41 00	-30 00 00	22/11/81	900	20.3
	U16903(f)	02 41 00	-30 00 00	24/12/95	900	20.7
	U16905(f)	02 41 00	-30 00 00	25/12/95	900	20.9
	U17248(f)	02 41 00	-30 00 00	13/09/96	900	21.2
f417	U15251	03 04 00	-30 00 00	27/11/92	1173	20.8
	U15273	03 04 00	-30 00 00	28/12/92	1800	21.5
	U15274(f)	03 04 00	-30 00 00	29/12/92	1800	20.3
	U16839(f)*	03 04 00	-30 00 00	22/10/95	900	-

The APM is a high speed micro-densitometer which is combined with a computer system which performs on-line image detection and analysis. The scanning laser samples a plate on a grid of positions at $\sim 8\mu$m separation. The detection algorithm identifies groups of connected pixels with densities higher than a given threshold above the local sky. This sky value is obtained from a preliminary scan, in which groups of 64×64 pixels are taken and the modal value found, these values produce the background map. The image analysis software then calculates a number of parameters for each image, including position, isophotal intensity, areal profiles and intensity weighted moments. These parameters were used in the next stage of analysis, which utilized the standard APM reduction software written by Dr. M. Irwin. The program `STATS` takes the moments, area and intensity of each image and uses them to perform a classification of images into noise, stellar, non-stellar and merged objects. Program `APMCAL` was then used to linearize stellar magnitudes and check the classification process. Multiple plate scans from the same field area were then combined using `MERGE`, and the astrometry was matched to the B1950 coordinates of the PPM astrometric catalogue (Bastian & Roeser, 1993) using `CHECK`.

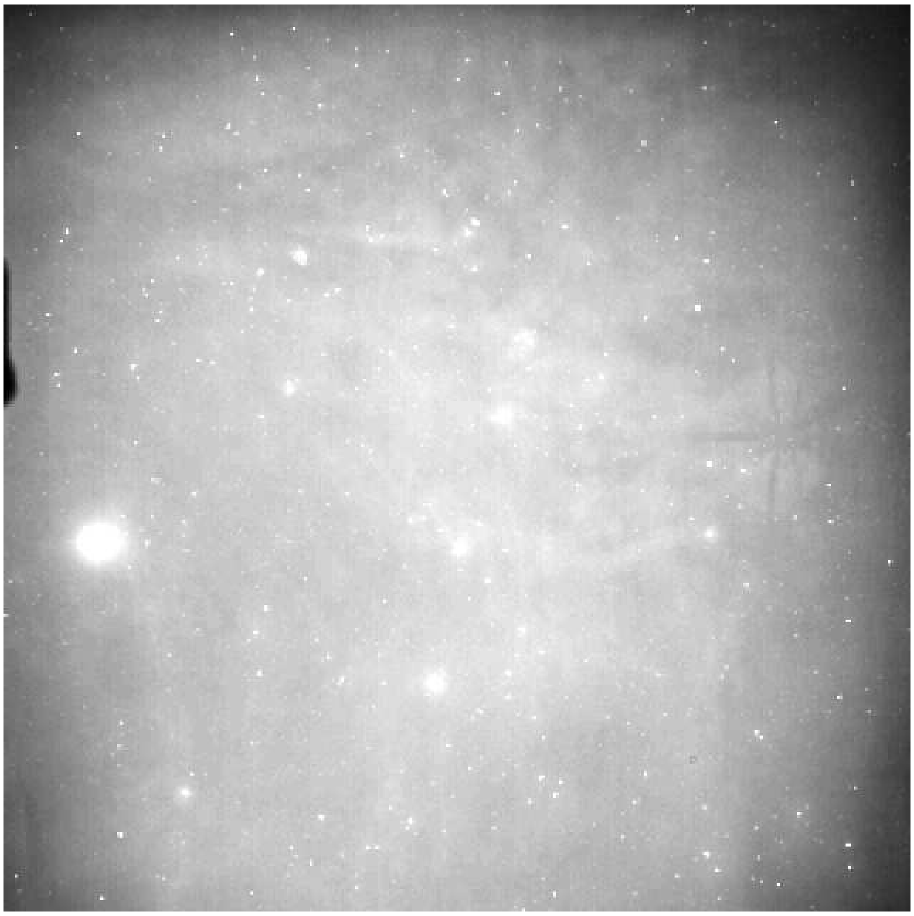

Figure 4.1: Background map for the APM scan of UKST plate *J4606c* in the F411 field. On the far left the effect of a step wedge can be seen. A number of bright stars are also obvious.

4.2.1 Correcting field effects on photographic plates

The APM measures a $\sim 5.8^{\circ} \times 5.8^{\circ}$ region of each UKST plate or film. Ideally we would use the whole of this area to construct the UVX catalogue, however, various *field effects* which are a function of position on the plate make this impossible; we use the central $5^{\circ} \times 5^{\circ}$ in construction of the catalogue. These field effects have two main sources, the first is the geometric vignetting of the telescope, causing a decrease in throughput for images which are progressively further off-axis. The second contribution is from *variable desensitisation* (Dawe & Metcalfe, 1982); the III-aJ emulsion is hypersensitized by soaking in hydrogen and nitrogen gases, a process which is gradually reversed by the action of water vapour and oxygen in the atmosphere. The UKST plate holder allows greater circulation of air at the plate edges, and so desensitisation occurs preferentially at these edges. The plate holder was modified in 1982, so that the plate surface was flushed with nitrogen gas during exposures. However, all the J plates used for the Southern UVX catalogue were taken before this upgrade.

The threshold for each scan is set to a constant value above the local sky value.

Therefore, in areas of strong vignetting, objects begin to fall below this threshold (a more correct method would be to define the threshold as a fractional value above the local sky, if the true sky intensity did not vary appreciably across the plate), and intensities are systematically reduced. Therefore a correction to the image intensities as a function of plate position needs to be made. This was done in the case of the APM Galaxy Survey (Maddox, 1988) by using the correlation between sky intensity (from background maps) and object numbers averaged over a large number of plates. A background map of an APM scan clearly shows the field response function. Fig. 4.1 shows the background map for plate J4606c in the f411 field, where the vignetting towards the corners is particularly obvious.

The final catalogue will only contain objects classified as stellar by the APM software. To correct the b_J stellar magnitudes for the field response function we have developed a method based on that of Maddox (1988). Below I will outline this process which was produced in collaboration with Robert Smith at the Institute of Astronomy, Cambridge, who developed a large fraction of the software for this correction procedure:

1. The number density of stellar objects increases as magnitudes become fainter, fitting this function allows us to relate the change in number density to a magnitude correction. We fit a quadratic function to the data in magnitude-Log(number) space, where the magnitudes are APM instrumental magnitudes, $m_{\rm APM} = 2.5\log(\text{APM intensity})$. At the plate edges the number-magnitude relation will be altered by the field effects that we are trying to correct, so only the central $4^\circ \times 4^\circ$ of each plate is used for finding the relation.

2. There are several regions on each plate which could not be used, mostly due to the halos of bright stars. Data in these areas were cut out of the sample and not used at any stage in the analysis, as they would be likely to have both erroneous magnitudes and background densities.

3. Each scan of our III-aJ plates was divided into a 32×32 grid. The number density of stellar objects in each of these grid cells was measured in magnitude bins (spaced logarithmically to obtain similar numbers of stars in each bin). The background density for the cell was also measured from a median filtered (to remove bright stars, see Fig. 4.1) background map of the scan. The number density was converted to a magnitude correction, relative to the centre of the plate using the number-magnitude relation.

4. The magnitude variation vs. background density data from each plate was then combined into one data set. This has the effect of removing any real structure in the stellar distribution, which, although less than that shown by galaxies (Maddox, 1988), would have a significant effect if the correction had been attempted on a plate by plate basis. A smooth surface is then fitted to the data, to obtain a correction which is dependent on both magnitude and background. All thirty III-aJ plates were combined in this process, 15 from the southern strip and 15 from the north. It was found that 3 plates in the Southern region (J5113, J6138 and J3818 in the f466, f471 and f417

fields respectively) showed a correlation that was significantly different from the plates in the rest of the sample. Data for these three plates were combined separately from the other 27 plates, and used to correct the plates in question.

5. The QSO candidates were to be selected on the basis of $u - b_J$ colour. To remove any residual vignetting and to correct any colour gradient in the plates we correct the u magnitudes, such that the distribution of colours over the area of the plate is uniform.

6. After the photographic magnitudes were calibrated (see below), the u magnitudes from individual plates were co-added, in order to reduce the r.m.s scatter in the u band photometry.

A detailed description of this process can be found in Smith (1997) .

4.2.2 CCD photometry of stellar sequences

Accurate photometric calibration is of vital importance in a survey of this kind, where colour is the basis of the selection procedure. In order to obtain this calibration we have observed a number of deep CCD sequences covering all of the Southern 2dF fields (similar data were obtained for the Northern survey area).

Observations of all the sequence fields were carried out using the Tek#3 CCD mounted at Cassegrain focus on the 0.9m telescope at Cerro Tololo Inter-American Observatory (CTIO) in two separate observing runs, from 23 – 27 August 1995 (observers: A. Ratcliffe and Q.A. Parker) and 15 – 20 September 1996 (observer: S.M. Croom). The Tek#3 CCD is a 2048×2048, thinned, AR coated device with low read noise and good QE in the U band. Readout is controlled by the ARCON system, which has four separate amplifiers allowing quad readout, giving quick readout times, $\sim$ 40s. The pixel scale is 0.396 arcsec pixel^{-1} giving a large $13.5' \times 13.5'$ field of view, allowing us to obtain magnitudes for a large number of stars $\sim$ 100 in each frame. The specific sequence areas were chosen to have a broad range of stellar magnitudes. During the first observing run B and R sequences were obtained for 14 of our 15 fields. During the second run we obtained $UBVR$ sequences in three fields including the one field previously unobserved, a list of fields observed is given in Table 4.3. Filters used for these observations were the standard CTIO $UBVR$ 3×3 inch filters, BVR being similar to the Harris BVR set, U uses a Copper Sulphate solution blocker. Magnitude zero-points, extinction and colour terms relating the instrumental magnitudes to the standard Johnson-Kron-Cousins system were obtained from frequent observations of standard stars from the E-field standards at $\delta = -45°$ (Graham, 1982). All observations of the sequence fields were made at low airmass, $\sec(z) \leq 1.34$.

Removal of the instrumental signature of the CCD from the images was carried out using the **ared.quad.quadproc** and **imred.ccdred.ccdproc** tasks in the IRAF package. **quadproc** is a variant of **ccdproc** specifically designed to reduce data from

Table 4.3: Data on all CCD sequence fields. $B_{\rm lim}$ is the limiting magnitude for 0.05mag photometric errors.

Field name	R.A.(B1950)	Dec. (B1950)	date	bands	$B_{\rm lim}$
f466-1	21 53 09.0	-29 33 46.0	24/08/95	BR	21.1
f467-1	22 06 17.0	-27 39 23.0	26/08/95	BR	20.7
f468-1	22 29 37.0	-31 27 40.0	25/08/95	BR	20.9
f469-1	23 03 00.0	-30 55 14.0	25/08/95	BR	21.2
f470-1	23 16 59.0	-29 47 52.0	25/08/95	BR	20.8
f471-1	23 45 03.0	-28 25 09.0	25/08/95	BR	21.2
f409-1	23 58 39.0	-27 50 31.0	25/08/95	BR	21.1
f410-1	00 34 16.0	-29 48 05.0	26/08/95	BR	21.0
f411-1	00 48 54.0	-28 46 39.0	26/08/95	BR	21.2
f412-1	01 14 27.0	-28 50 55.0	26/08/95	BR	20.8
f413-1	01 32 06.0	-31 53 51.0	26/08/95	BR	20.8
f414-1	02 04 19.0	-28 32 57.0	25/08/95	BR	21.2
f415-1	02 18 38.0	-32 07 57.0	24/08/95	BR	21.2
f417-1	03 10 24.0	-28 01 59.0	26/08/95	BR	21.2
f466-2	21 51 23.0	-30 05 00.0	15/09/96	$UBVR$	20.8
f409-2	00 00 23.0	-29 38 59.0	15/09/96	$UBVR$	20.8
f416-2	02 45 24.0	-30 31 00.0	15/09/96	$UBVR$	20.9

the multi-readout ARCON system. This software removes the instrumental bias and also corrects bad columns and pixels (of which there are a number in the Tek#3 CCD) as well as flat fielding each frame. In each passband we obtained both dome flats taken during the day and sky flats taken at twilight. It was found that both dome and sky flats adequately corrected small scale variations in pixel sensitivity. However, division by dome flats generally left a residual large scale gradient across the image. This gradient was at the 5% level in many cases, therefore we used the sky flats, which flattened the images to the 1% level. At least 5 separate exposures were used to generate each flat-field. These were median combined using 3σ clipping to remove cosmic ray events (CREs).

We used the IRAF task **digiphot.daophot.phot** to obtain photometry of all the E-field standard stars observed. We used 25-pixel ($10''$) radius apertures centred on each standard star to obtain their instrumental magnitudes, which we denote by $U_{\rm CCD}$, $B_{\rm CCD}$, $V_{\rm CCD}$ and $R_{\rm CCD}$; the instrumental magnitude is simply,

$$m_{\rm CCD} = -2.5\log(f) + 2.5\log(t) \tag{4.3}$$

where f is the flux and t the exposure time. The sky background value was obtained from the mode of an annulus between 35 and 50 pixels in radius. The IRAF task **digiphot.photcal.fitparams** was used to obtain the magnitude zero-points, colour and extinction terms. For the first set of data (BR sequences) we assumed standard extinction values for Cerro-Tololo: $A_{\rm B}$ = 0.209 mag airmass^{-1}, $A_{\rm R}$ = 0.108 mag airmass^{-1}. For these data the maximum airmass reached was 1.341 in $R_{\rm CCD}$ and 1.292 in $B_{\rm CCD}$, with over 50% of the observations obtained at airmasses of less than 1.1; therefore even in the most extreme cases this assumption would cause a zero-point error of less than 0.01 mag. For the second set of data ($UBVR$ sequences) we calculated the extinction terms from the standard observations made; these were $A_{\rm U}$ = 0.453 mag airmass^{-1}, $A_{\rm B}$ =0.232 mag airmass^{-1}, $A_{\rm V}$ = 0.131 mag airmass^{-1} and $A_{\rm R}$ = 0.113 mag airmass^{-1}. Inverse colour equations were fitted giving

$$\begin{aligned} B_{\rm CCD} &= B - 22.442 + 0.209\sec(z) + 0.095(B-R) \quad \text{r.m.s.} = 0.003 \\ R_{\rm CCD} &= R - 22.566 + 0.108\sec(z) + 0.006(B-R) \quad \text{r.m.s.} = 0.004 \end{aligned} \tag{4.4}$$

for the first set of observations while the second set of observations gave

$$\begin{aligned} U_{\rm CCD} &= U - 20.240 + 0.453\sec(z) - 0.035(U-B) \quad \text{r.m.s.} = 0.014 \\ B_{\rm CCD} &= B - 21.800 + 0.232\sec(z) + 0.110(B-V) \quad \text{r.m.s.} = 0.014 \\ V_{\rm CCD} &= V - 22.030 + 0.131\sec(z) - 0.019(B-V) \quad \text{r.m.s.} = 0.007 \\ R_{\rm CCD} &= R - 21.992 + 0.113\sec(z) - 0.002(V-R) \quad \text{r.m.s.} = 0.005 \end{aligned} \tag{4.5}$$

The sequence fields were combined using **imcombine** with the **crreject** algorithm used to reject CREs. In the case of single exposures on a field (as was the case for data from the first run), we used the image detection routines, and the matching of images in different bands to reject cosmic ray events. All images with peak counts higher than a 5σ threshold above the sky background were selected using **daofind**. Aperture photometry was obtained for these objects using **phot** within 10 and 25 pixel apertures. The larger aperture, corresponding to 10″ radius, is the same as that used for our standard observations and defines the zero-point for our magnitude system. The median seeing during the observations was 1.5″ and was rarely above 2.0″. At faint fluxes the sky counts add considerable noise within an aperture of this size. For this reason we obtained magnitudes within a 10 pixel aperture and then corrected this magnitude to the 25 pixel magnitude scale using the brightest unsaturated stars (at least 8 per field) with no close companions in each field to define the aperture correction, which was typically $\sim$ 0.03 mag. The aperture corrected instrumental magnitudes were then converted to the standard $UBVR$ system using the **invertfit** task and the colour equations derived above. The Poisson photometric errors were plotted as a function of magnitude (e.g. Fig. 4.2) in order to estimate the effective limiting magnitude of the standard observations in each field (in this case the magnitude at which the photometric errors reach 0.05 mag). The limiting B band magnitudes are shown in Table 4.3.

The brightest 10 unsaturated stars in each field were matched to their positions on the APM scans of the UKST III-aJ survey plates which in turn have been matched to the PPM (B1950) (Bastian & Roeser, 1993) astrometric catalogue. These stars were then used to derive a transform from CCD (x, y) positions to (α, δ) using the STARLINK ASTROM software.

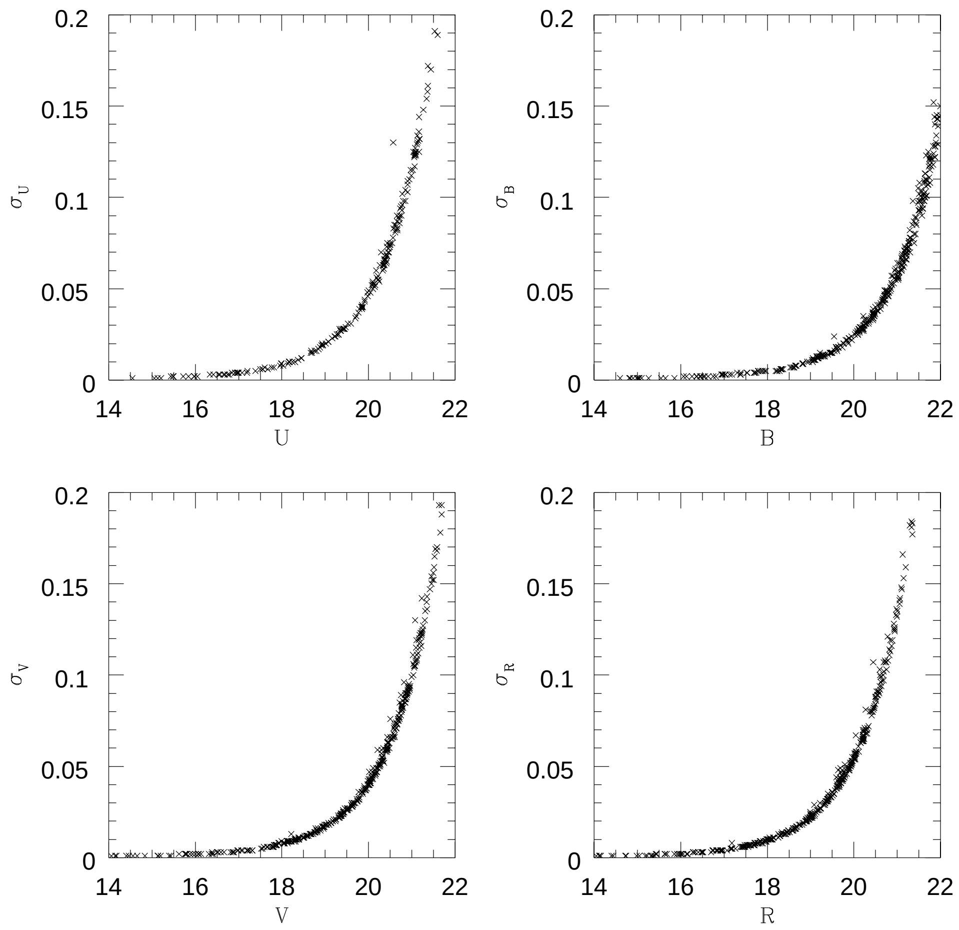

Figure 4.2: Poisson photometric errors for $UBVR$ bands in the f466-2 CCD field.

4.2.3 Calibrating photographic plates with CCD sequences

We obtain an equivalent calibrated b_J magnitude for each target CCD star using the colour equation in Eq. 4.1. In the case of data from the first run, in which we only observed in the B and R bands it was first necessary to convert the colour term from $(B-V)$ to $(B-R)$, which was done using the relation

$$(B-R) = 1.54(B-V) \tag{4.6}$$

(Metcalfe et al., 1991), which was derived from the Landolt (1983a,b) standard stars. Fig. 4.3 shows this relation plotted against the E-Field standards used in our observations. All the objects with b_J magnitudes in our CCD fields were matched to the APM scans of the III-aJ plates. The objects classified as stellar on the scans were taken and the relation between $m_{\rm APM}$ (after being corrected for field effects) and $b_J(CCD)$ was fitted with a quadratic function. This function was used to convert the non-linear instrumental photographic magnitudes to the linear magnitude system. The data and fits for all 15 Southern III-aJ plates are shown in Fig. 4.4. To obtain a

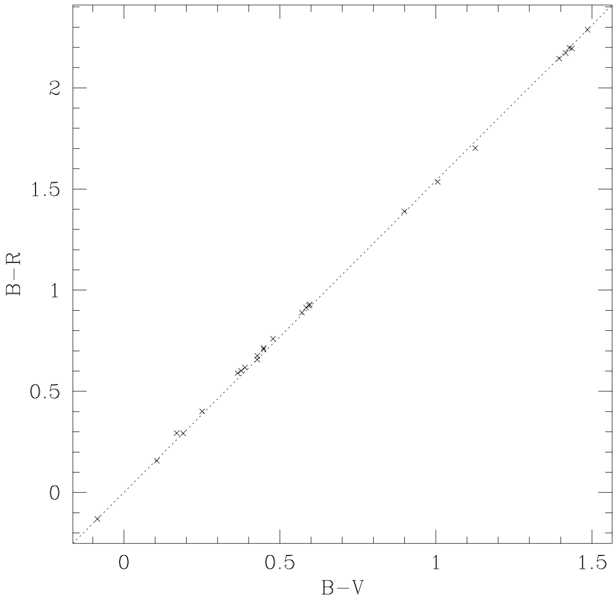

Figure 4.3: Plot of $(B - R)$ vs. $(B - V)$ colour for the E-Field standard stars used. The dotted line is the relation in Eq. 4.6.

uniform photometric system over each survey strip we then attempted to match the calibrated magnitudes in the overlaps between each plate, and correct the individual plate zero-points to obtain a zero-point defined by the f470/f471 plates which have the smallest offsets of any plate pairing. The zero-point offsets for all plates are listed in Table 4.4. It is possible that this process will actually add systematic errors to the survey photometry, as it utilizes the poorer areas of the photographic plates to obtain the relative plate zero-points. Below we shall make several checks to ascertain if this is the case, before deciding whether to use the overlap corrections or direct CCD calibration in the final catalogue. In the first instance we will simply use the direct CCD calibration.

Until now we have only discussed the photometric calibration of the III-aJ plates. It is obvious from Table 4.3 that we do not have $U_{\rm CCD}$ sequences in all of our survey fields. However, these are not necessary in order to calibrate the photographic u band photometry. In each field area we have several tens of thousands of stellar images with both u and $b_{\rm J}$ magnitudes. A large fraction of these images are blue galactic stars which follow a straightforward relation in the $(u - b_{\rm J})$ vs. $b_{\rm J}$ plane. This blue stellar ridge-line has been shown to remain at a constant $(u - b_{\rm J})$ colour as a function of $b_{\rm J}$ magnitude (Boyle, 1986). We shall assume $(u - b_{\rm J})_{\rm ridge-line} = 0$; this is probably correct to ± 0.2 mag. Fitting this relation allows us to bootstrap from our $b_{\rm J}$ magnitudes to obtain a photometric zero-point in our u band. It can be seen from Table 4.2 that we have several available u plates in each UKST field area. To improve the r.m.s. error in the photographic magnitudes, particularly at magnitudes near to the plate limit, we co-add the calibrated intensities of matched objects for all plates which reached a depth of at least $u = 20.8$ in each field.

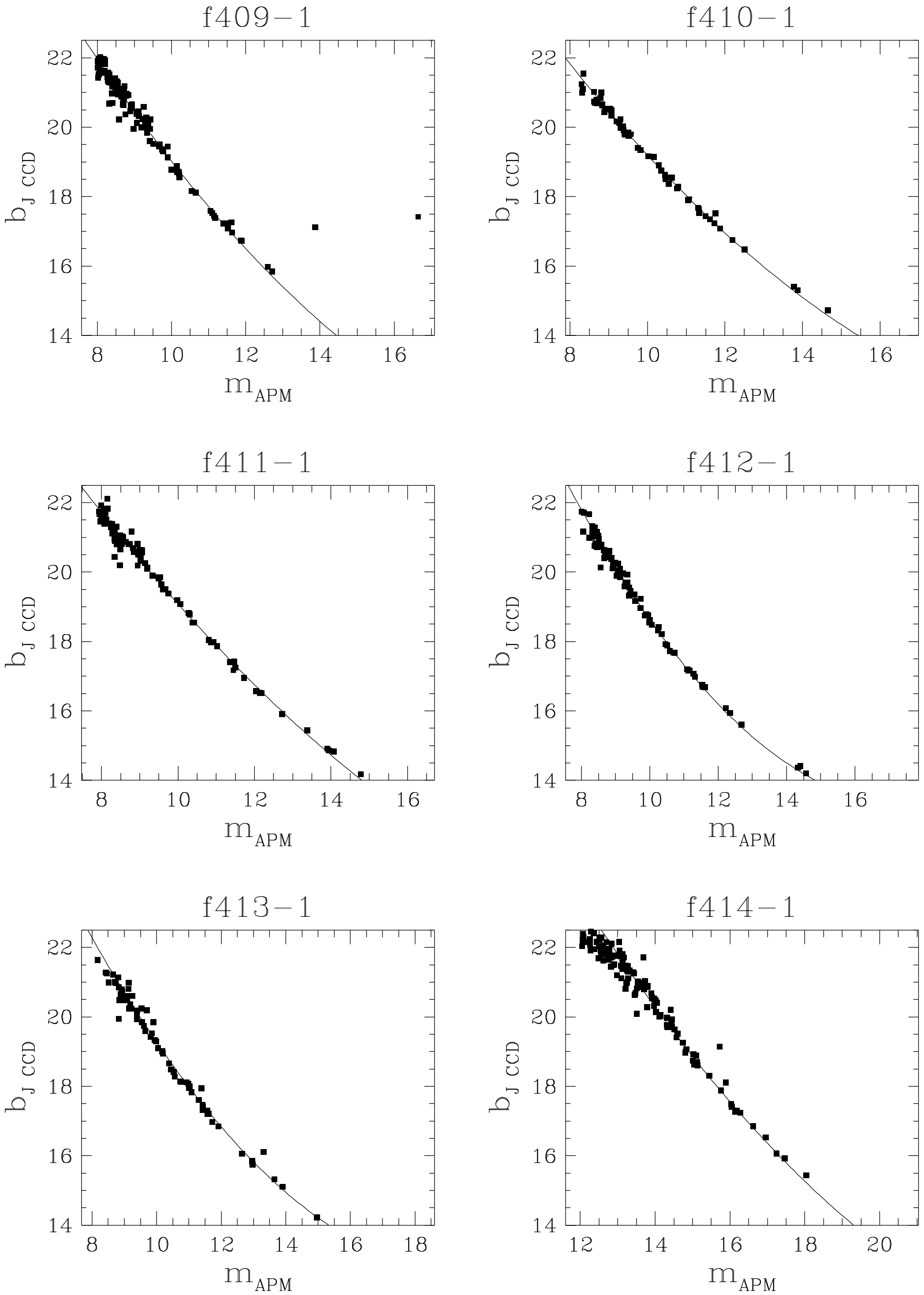

Figure 4.4: Plot of b_J CCD magnitude vs. APM instrumental magnitude for all the Southern b_J plates. The solid line shows the quadratic fit used to calibrate the APM magnitudes in each field.

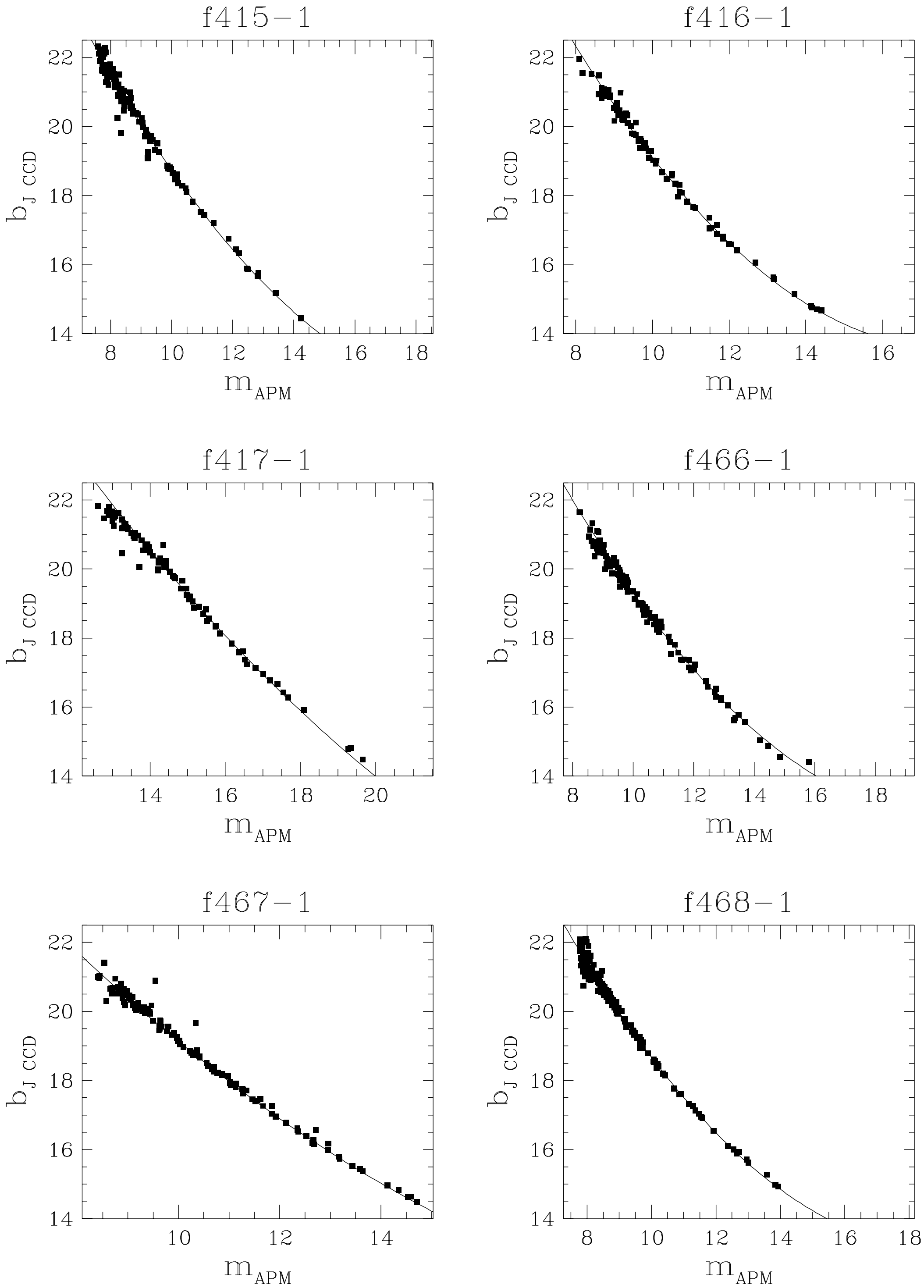

Figure 4.4: $b_{\mathrm{J\ CCD}}$ vs. m_{APM}: continued.

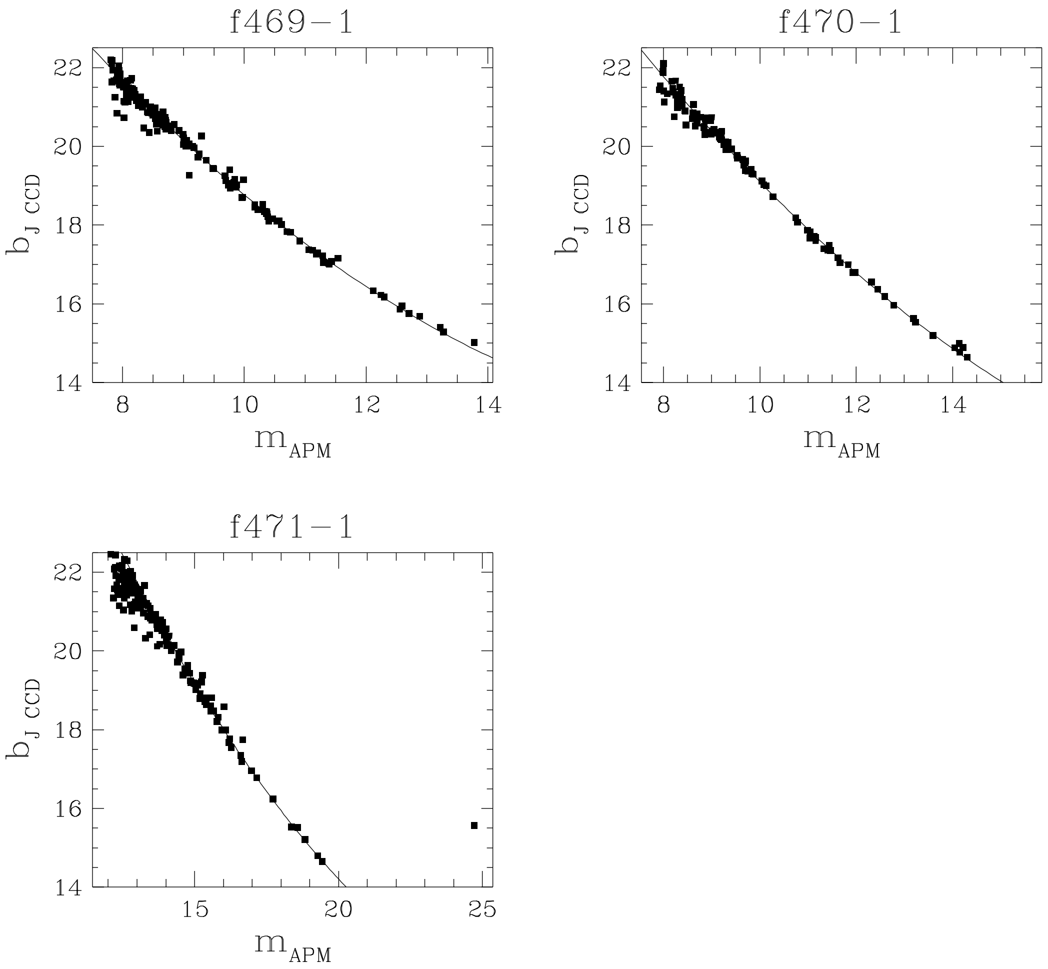

Figure 4.4: $b_{\rm J\ CCD}$ vs. $m_{\rm APM}$: continued.

4.2.4 Checks on the photometric calibration

In field f466 we have two sets of B CCD sequences. These allow us to directly confirm the accuracy of the zero-point used in this field, Fig. 4.5 shows a comparison of photographic magnitudes, calibrated by the f466-1 CCD sequence (i.e. not zero-point corrected using plate overlaps), with CCD magnitudes from the f466-2 field. The mean offset 0.048 ± 0.01 mag, is an estimate of the systematic variation of the photographic magnitudes in the f466 field. However, it should be noted that both f466-1 and f466-2 are situated towards the centre of the f466 field where systematic variations should be at a minimum. A more extensive program of CCD imaging would allow the systematic magnitude variations across the plates to be estimated before and after the field-effect correction procedure.

The U CCD photometry available allows us to test the accuracy of our u band zero-point and linearization obtained from the ridge-line fitting. We might expect that galactic reddening would cause the exact position of the ridge-line to vary

Table 4.4: The $b_{\rm J}$ offsets from plate-edge matching. The offsets were calculated from the mean offset of the stellar magnitudes matched in plate overlaps. Errors in the measured offsets are of the order ~ 0.004 mag.

Field name	$b_{\rm J}$ offset
f466	-0.062
f467	-0.101
f468	-0.043
f469	0.028
f470	0.000
f471	0.001
f409	-0.037
f410	0.038
f411	0.073
f412	-0.149
f413	0.084
f414	0.108
f415	0.270
f416	0.246
f417	-0.021

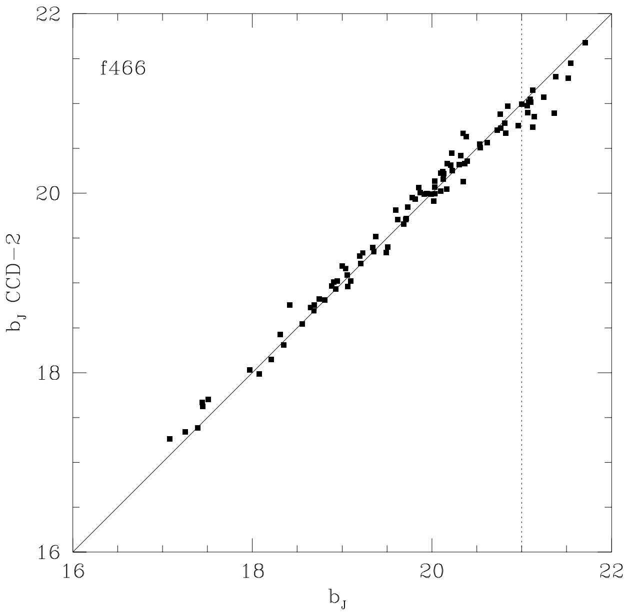

Figure 4.5: Comparison of the calibrated photographic $b_{\rm J}$ (from the CCD sequence f466-1) magnitudes in the f466 field and $b_{\rm J}$ magnitudes derived directly from the f466-2 CCD sequence.

systematically over our survey region. Using the simple relation of Woltjer (1975),

$$E(B-V) = 0.06\mathrm{cosec}|b_{\mathrm{II}}| - 0.06 \tag{4.7}$$

which relates reddening to galactic latitude, b_{II}, we expect a low level of reddening at both ends of the Southern strip. f466-2 ($b_{\mathrm{II}} = -51^{\circ}.22$) has $E(B-V) = 0.017$mag while f416-2 ($b_{\mathrm{II}} = -64^{\circ}.42$) has $E(B-V) = 0.007$mag. Reddening derived from HI and galaxy counts (Burstein & Heiles, 1982) also gives similar measures of $E(B-V) \simeq 0.01$mag. The reddening in $E(B-V)$ can be converted to a $(U-B)$ extinction using

$$\frac{E(U-B)}{E(B-V)} = 0.72 + 0.05E(B-V) \tag{4.8}$$

(Zombeck, 1990). It is clear that this gives a very small offset in the $(U-B)$ colours, with the difference in $E(U-B)$ from one end of the strip to the other being ~ 0.005 mag.

Fig 4.6 shows a comparison of ridge-line photometry with direct CCD photometry for two fields, f416 and f466, *without* zero-point corrections from plate-edge matching. The ridge-line photometry for both of these fields has almost exactly the same systematic zero-point offset with respect to the CCD photometry. The mean offset in the f466 field is 0.218 ± 0.018 mag, while f416 shows a 0.186 ± 0.020 mag offset. This therefore suggests that for these two fields the u ridge-line photometry is consistent to ± 0.03, with an offset of ~ 0.2 mag relative to the standard photoelectric U band. Further U CCD photometry will be required to confirm this over the rest of the survey area.

4.2.5 $u - b_{\mathrm{J}}$ selection of QSO candidates

The fully calibrated and flattened stellar catalogue was then used to select the final UVX catalogue which forms the candidate list for follow-up spectroscopy. For the reasons discussed above, and those outlined below, we did not use plate-edge matching to zero point the photometry in individual fields. Fig 4.7 shows colour-magnitude plots for all 15 of the fields in the Southern survey region. Also shown here are all the previously known QSOs (Veron-Cetty & Veron, 1996); we shall use these objects in Section 4.3 to make an estimate of the completeness of the survey. The 2dF survey limits are $18.25 < b_{\mathrm{J}} < 21.0$ (note, the FLAIR survey covers the range $17 < b_{\mathrm{J}} < 18.25$), and $(u - b_{\mathrm{J}}) \leq -0.36$. Within these limits there are ~ 22000 candidates covering an effective area of 355.4 deg^2. The colour limit was chosen to be the reddest limit possible given the faint limit of $b_{\mathrm{J}} = 21$ and a maximum surface density of candidates of $\sim 62 - 63$ per deg^2. This second constraint was a balance of practical observational considerations, and our desire to obtain a QSO catalogue with a high level of completeness. Below we will discuss the effectiveness of our chosen criteria and issues concerning the calibration of the survey.

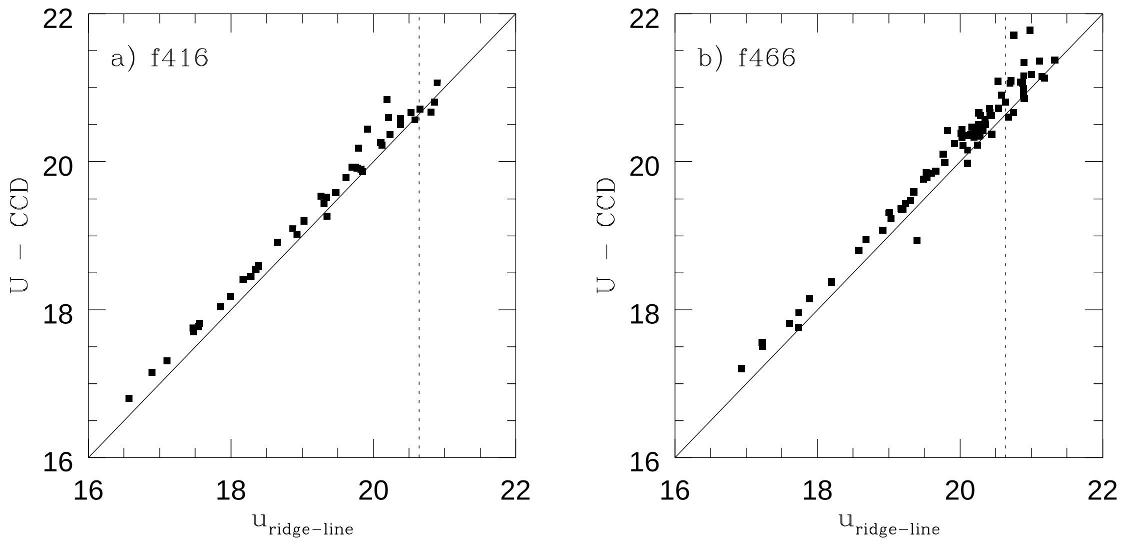

Figure 4.6: A comparison of U CCD photometry and u ridge-line photometry in two fields at opposite ends of the southern 2dF QSO survey strip, a) f416 and b) f466. The solid line is $U = u_{ridge-line}$, the dotted line corresponds to the chosen $u - b_J$ selection limit of $u - b_J = -0.36$ for $b_J = 21$.

4.3 Testing the UVX Catalogue

We now come to discuss the properties of the UVX catalogue in the Southern strip which is shown in Fig. 4.8. The most obvious feature is a significant number gradient across the survey area. This is more clearly shown by a histogram of UVX number density for consecutive fields (Fig. 4.9). Several fields show higher than average candidate densities; in f410, f413 and f415 it is likely that we are seeing an increased number of stars being scattered into our selection limits due to the relatively bright limiting magnitudes of the u plates in these fields, which are $u = 20.8 - 20.9$. f466 also has a large excess, and although this might be expected of the field closest to the galactic bulge it is likely that a small zero-point error could also increase the number. Fig. 4.9 also shows the number densities for each field after using plate edge matching. There is obviously a much larger gradient across the strip in this case. The zero-point offsets shown in Table 4.4 have been plotted in Fig. 4.10. There is a clear correlation between number density and zero-point correction. Of particular interest is the f412 field which has an excess with respect to the surrounding fields of ~ 10 deg^{-2} with plate edge matching, but has a deep u plate ($u_{\rm lim} = 21.2$). An excess of $\simeq 10$ deg^{-2} implies a zero-point offset of $\simeq 0.2$ mag assuming the number-magnitude relation has a slope of $\simeq 0.28$ (that is $N(m) \propto 10^{0.28m}$), which is in fact the offset relative to the f411 and f413 fields listed in Table 4.4. This is further evidence to suggest that plate matching leaves residual $\sim 0.1 - 0.2$ mag zero-point differences between the survey fields, and so is additional justification for not using plate-edge matching.

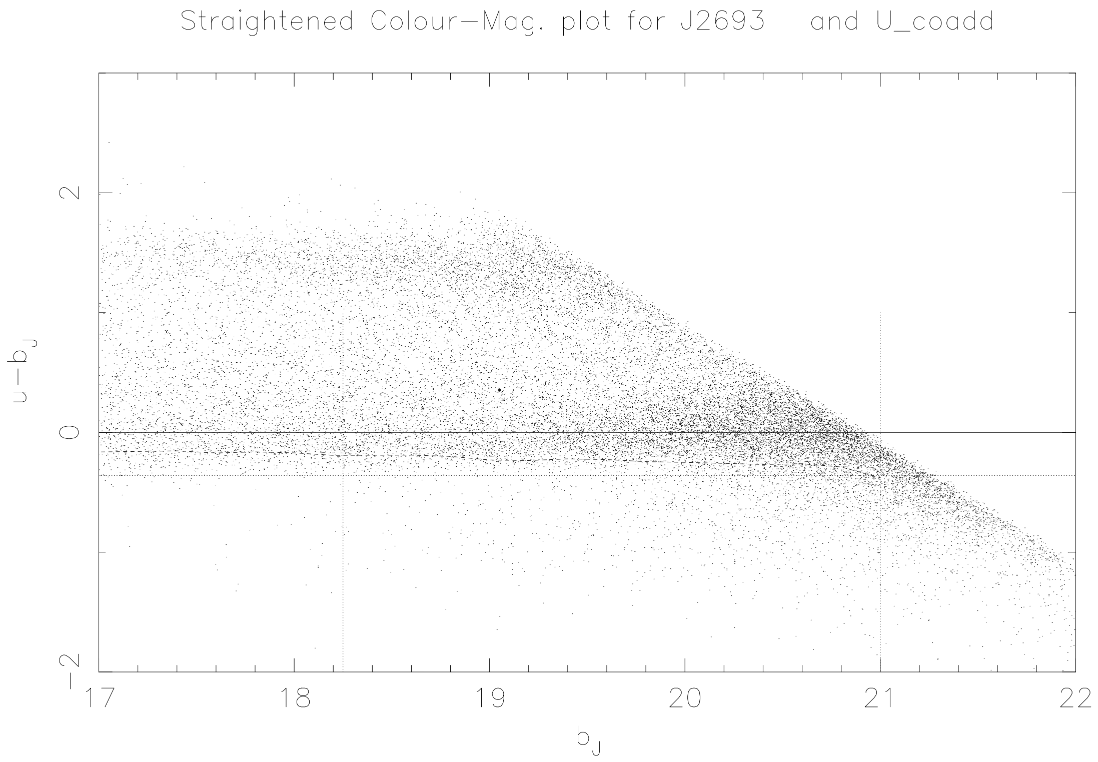

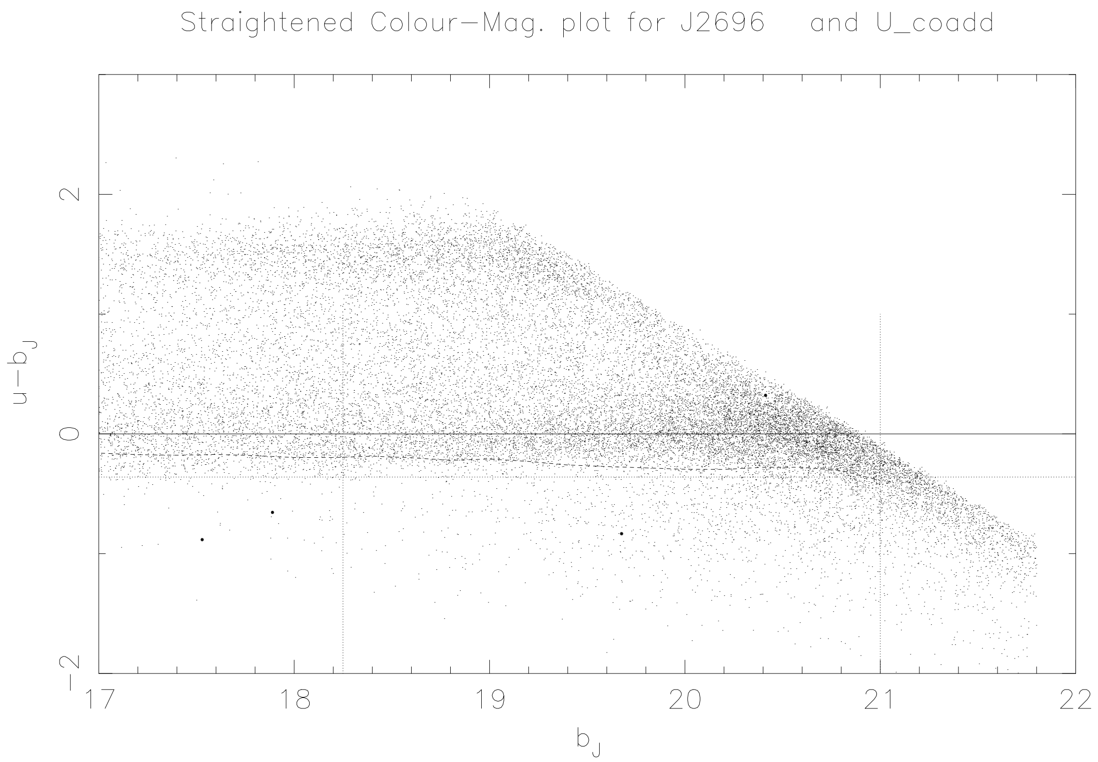

Figure 4.7: Colour-magnitude plots used to select UVX objects for each field in the Southern strip of the 2dF QSO survey. The solid lines show $u - b_J = 0$ and the survey limits of $u - b_J = -0.36$, $18.25 < b_J < 21.0$. The dotted line shows the FWHM of the stellar ridge-line. The large points show previously known QSOs.

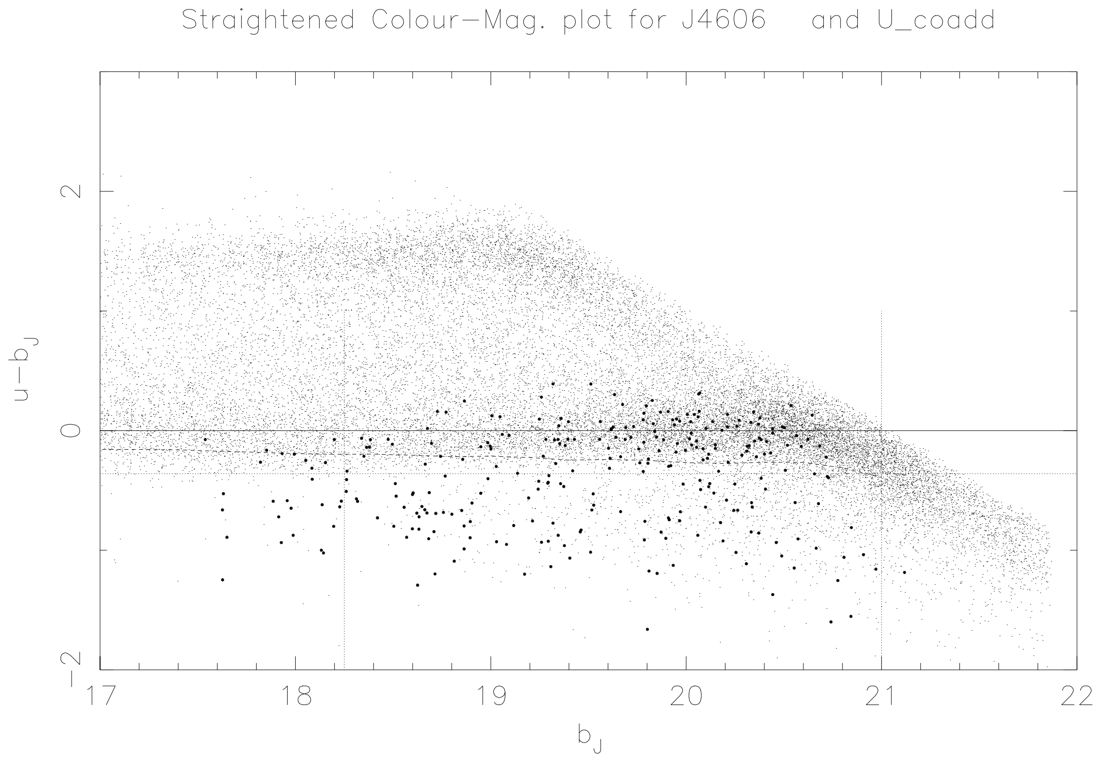

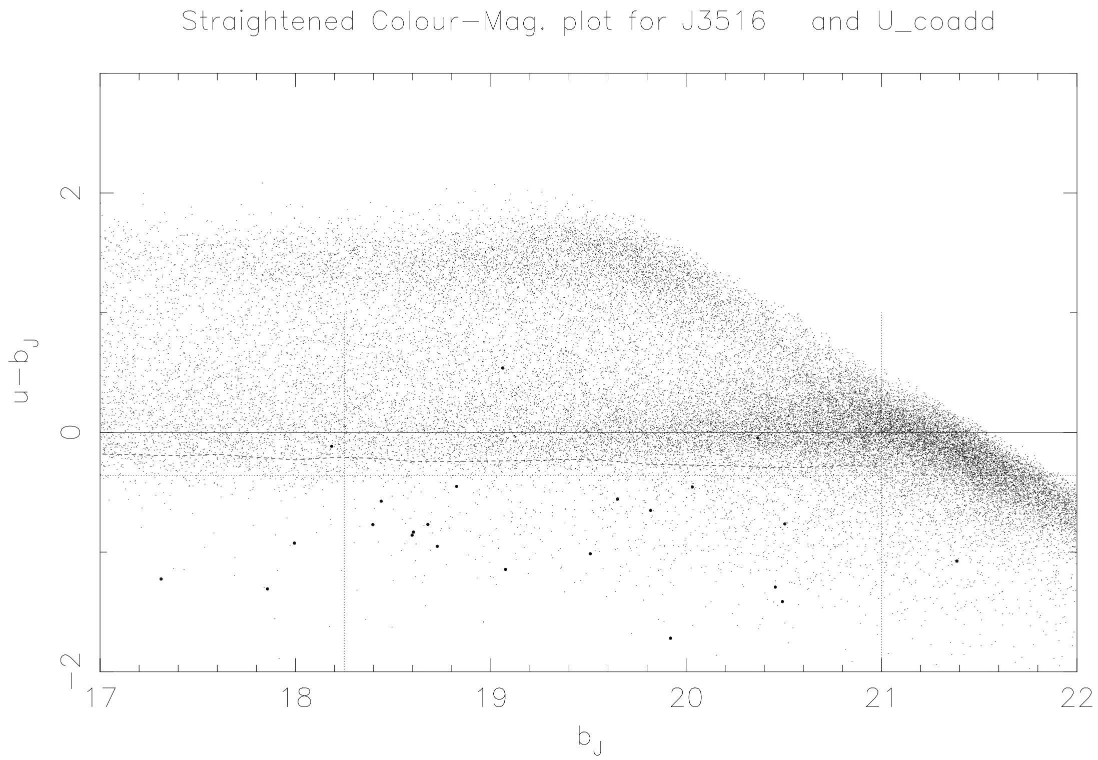

Figure 4.7: Colour-magnitude plots: continued

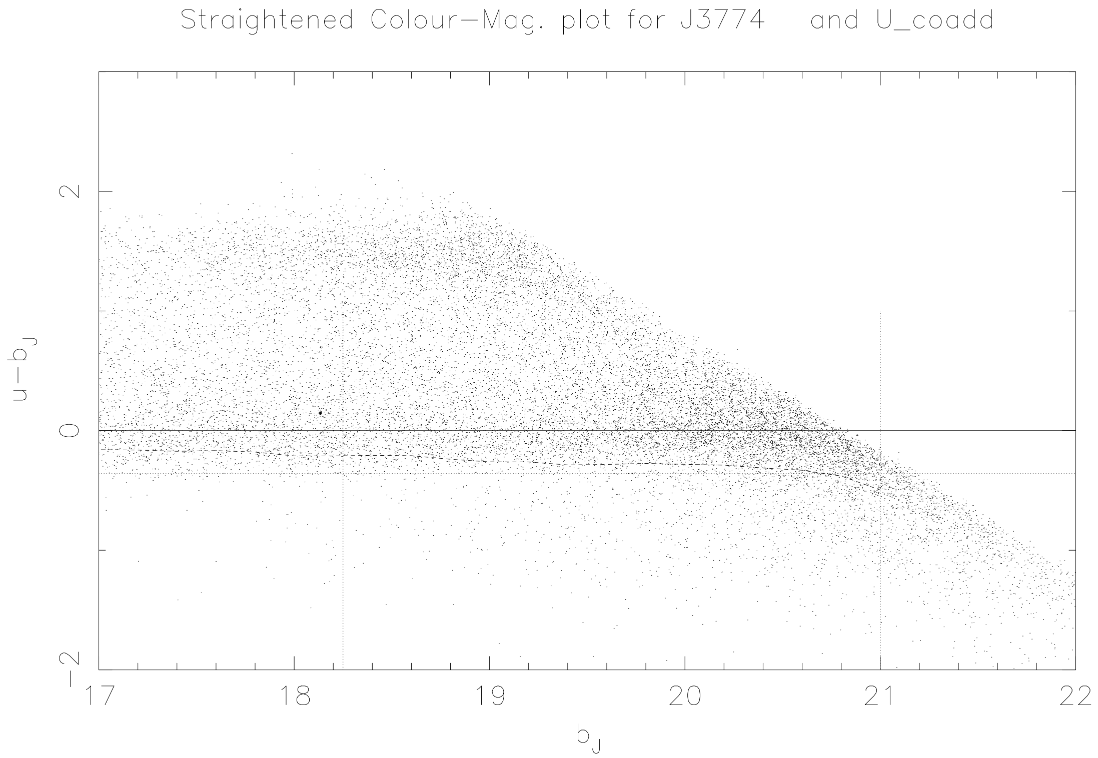

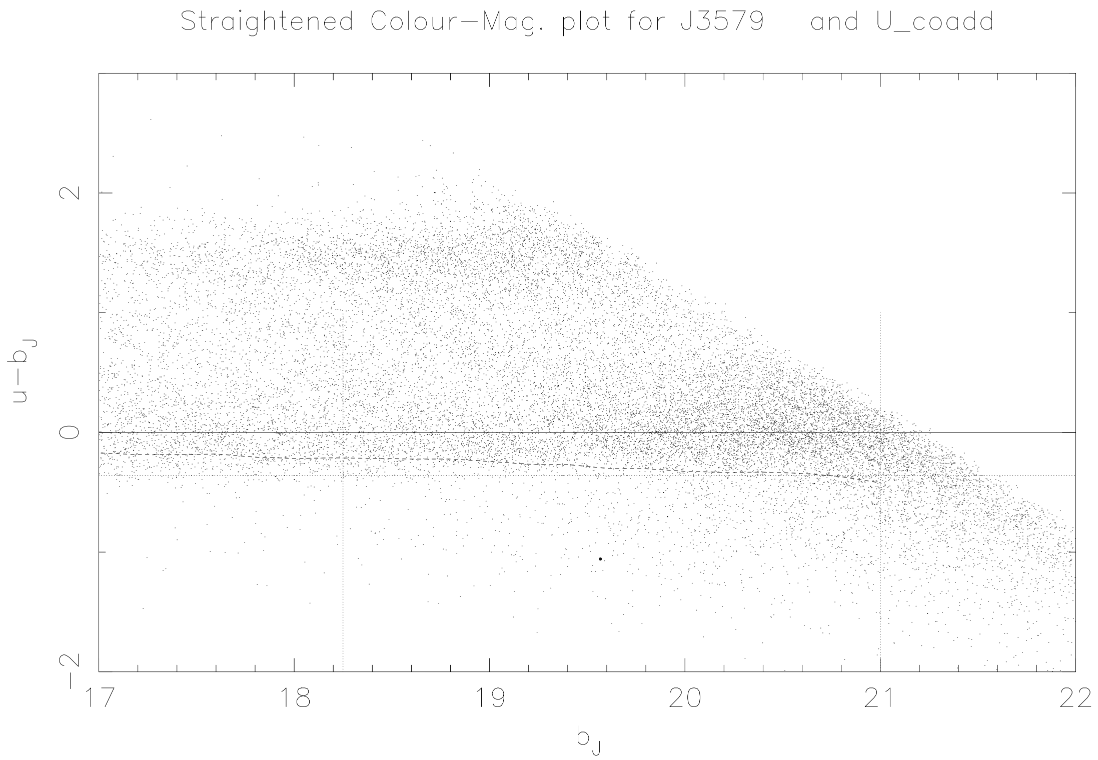

Figure 4.7: Colour-magnitude plots: continued

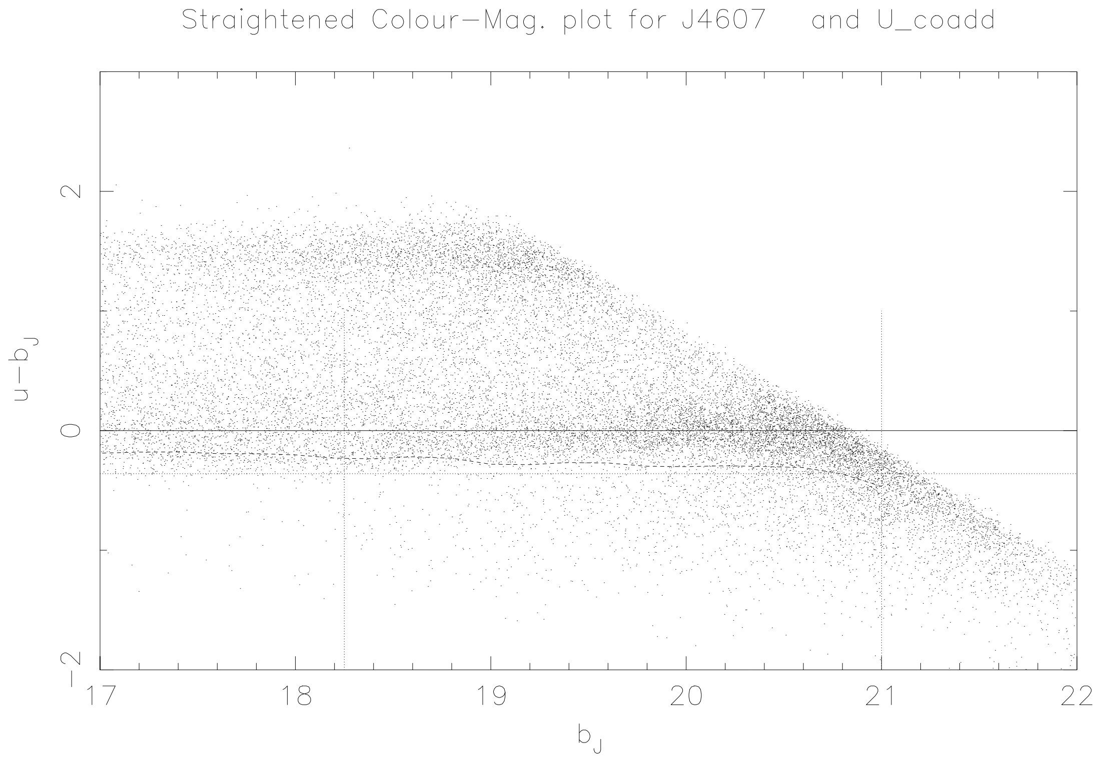

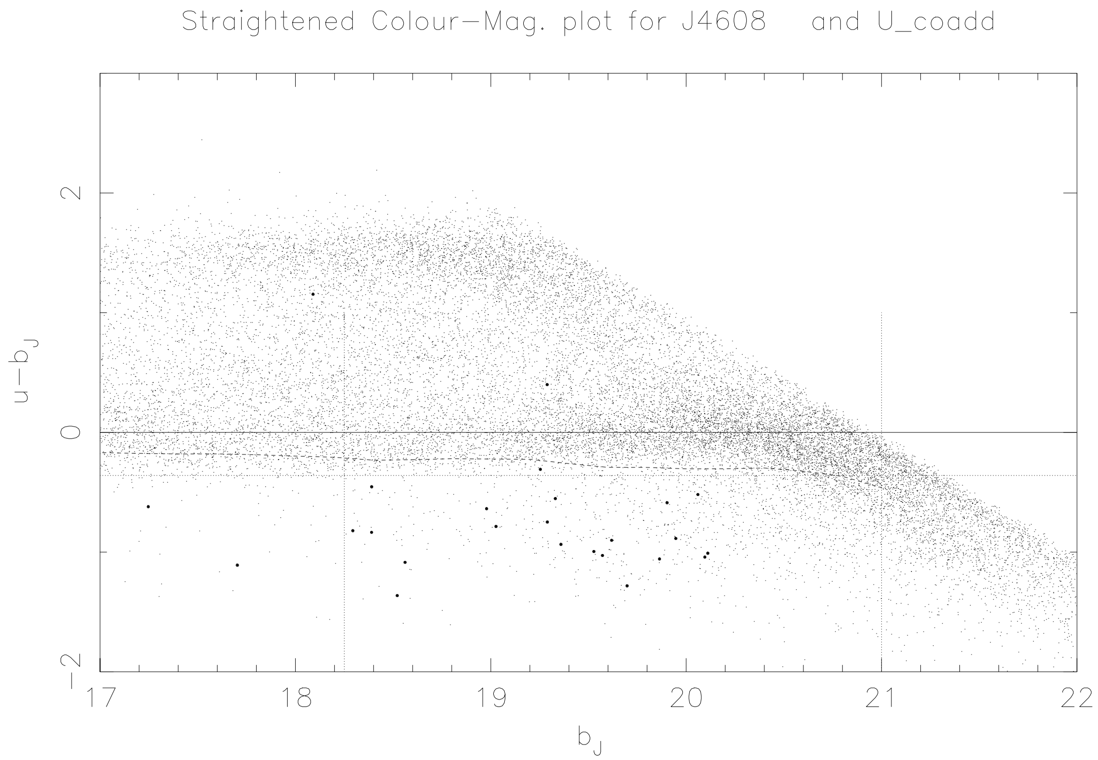

Figure 4.7: Colour-magnitude plots: continued

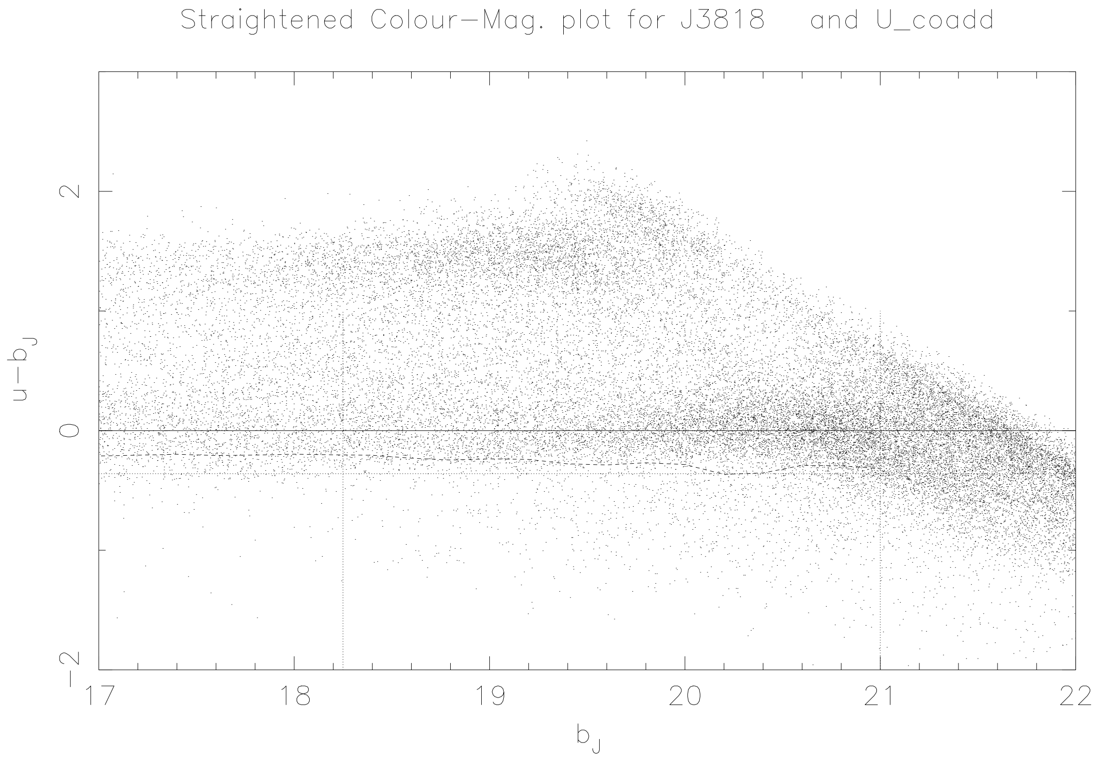

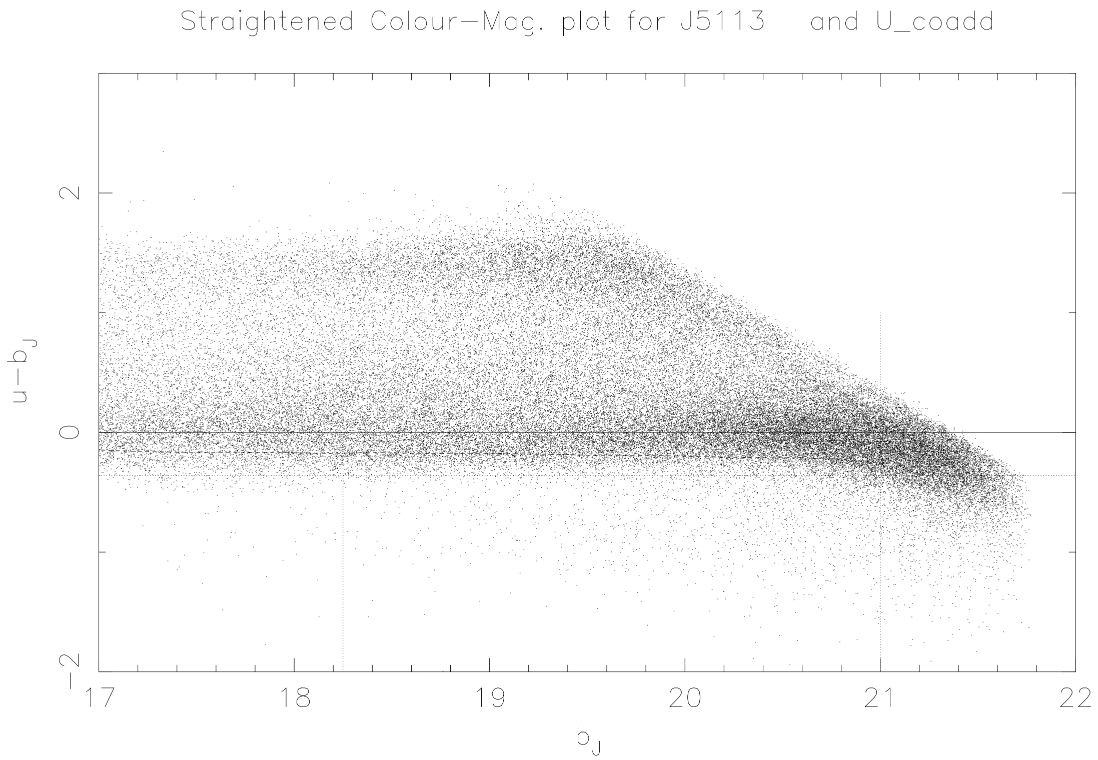

Figure 4.7: Colour-magnitude plots: continued

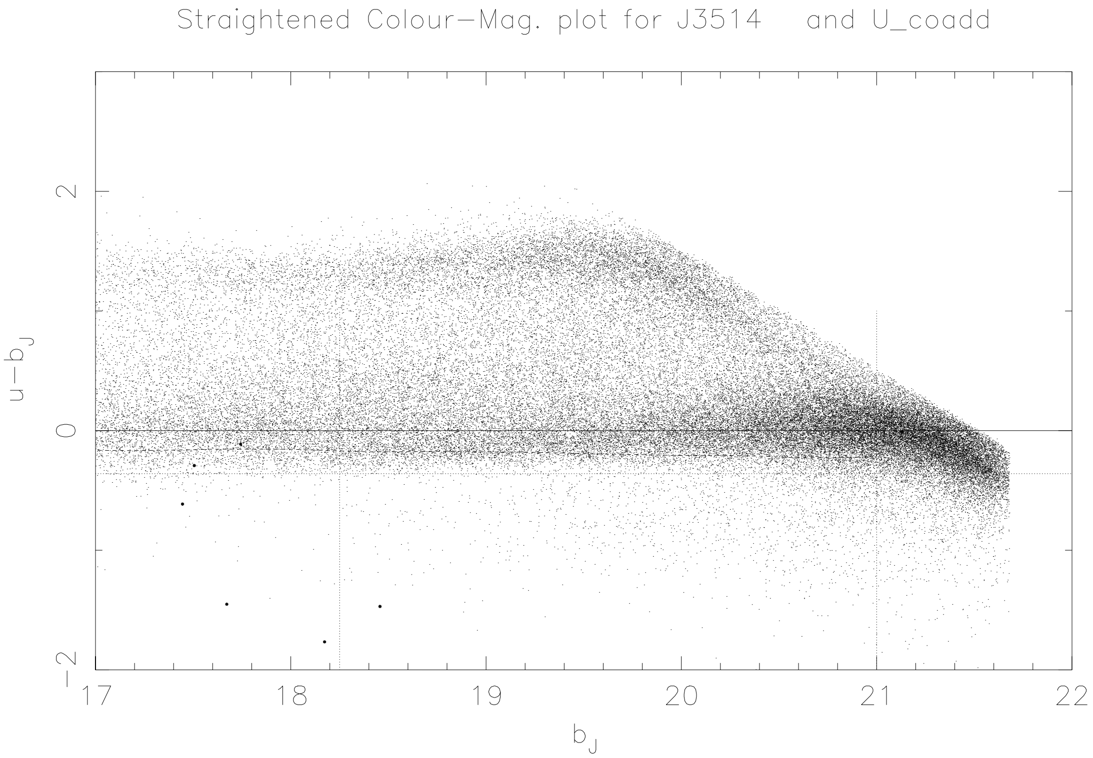

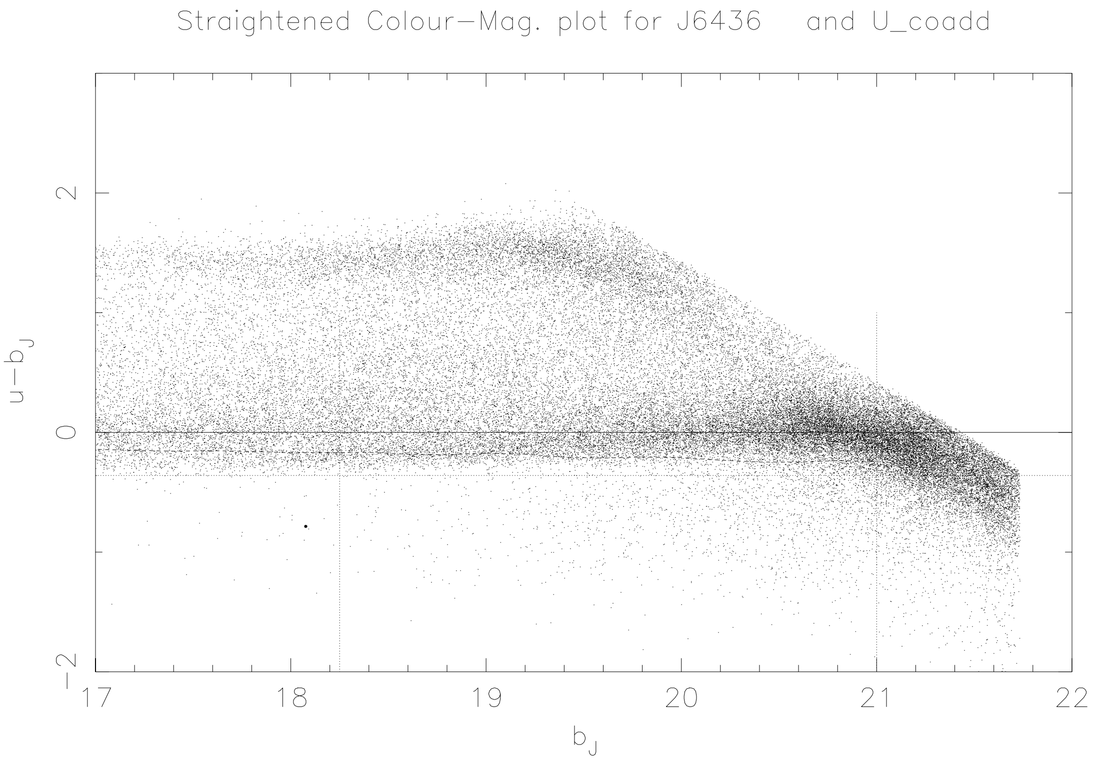

Figure 4.7: Colour-magnitude plots: continued

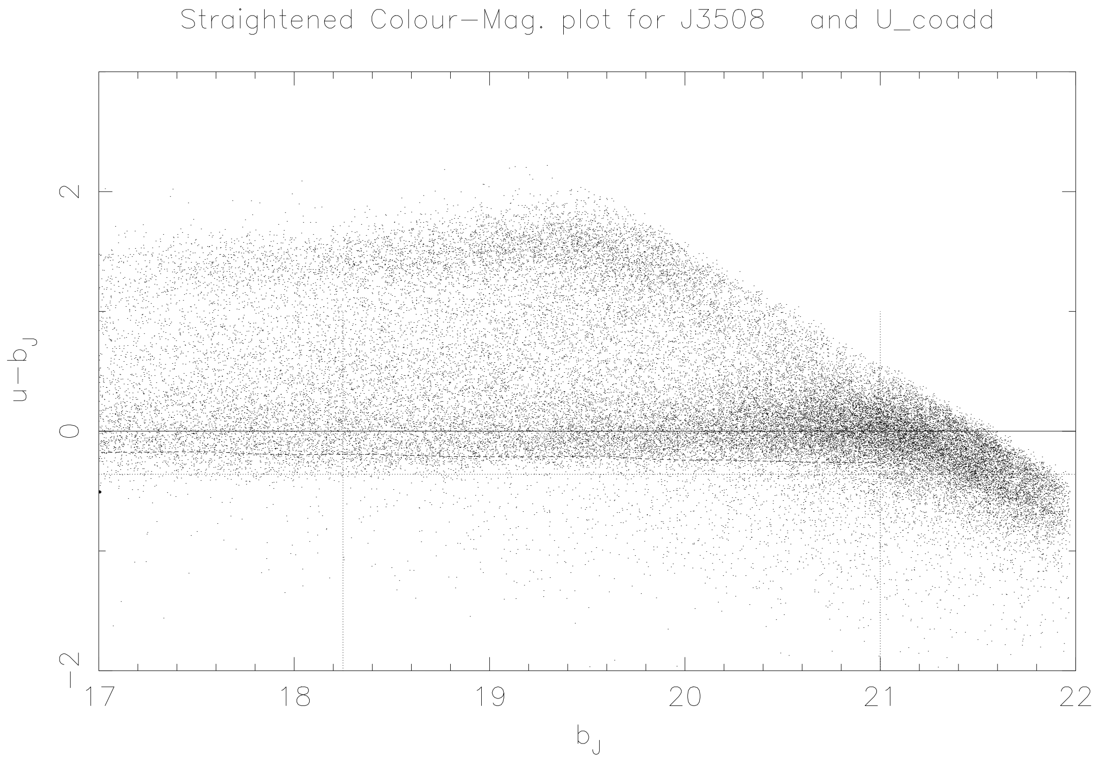

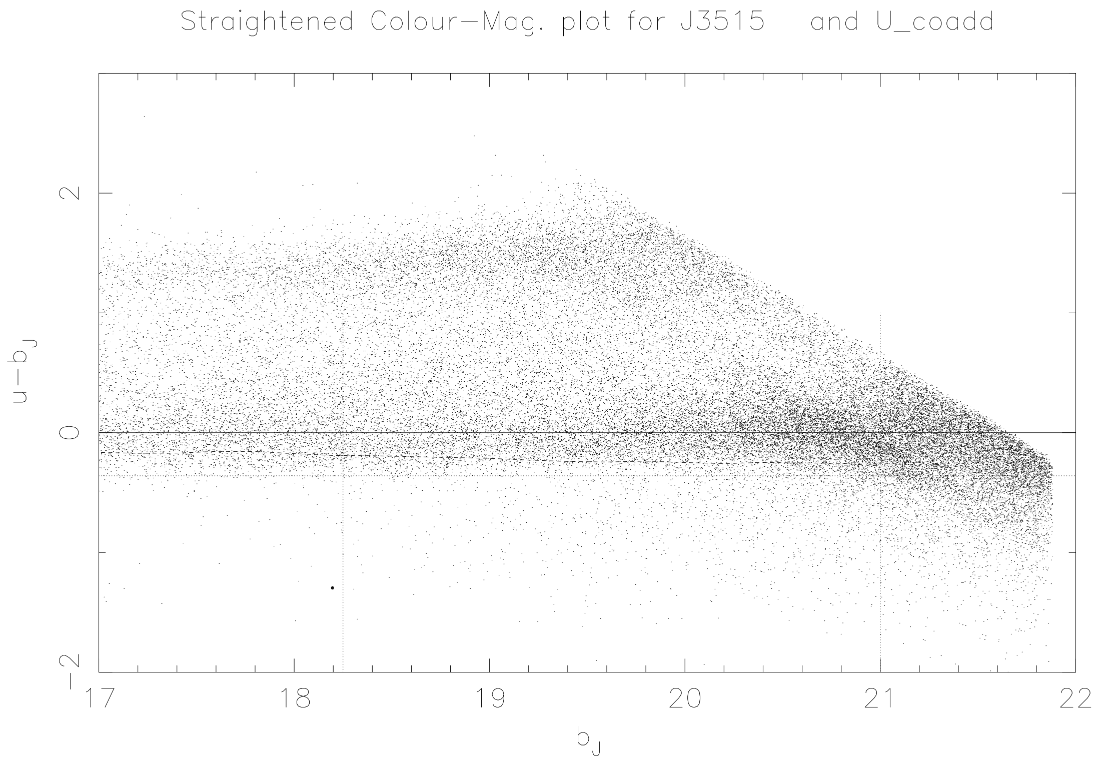

Figure 4.7: Colour-magnitude plots: continued

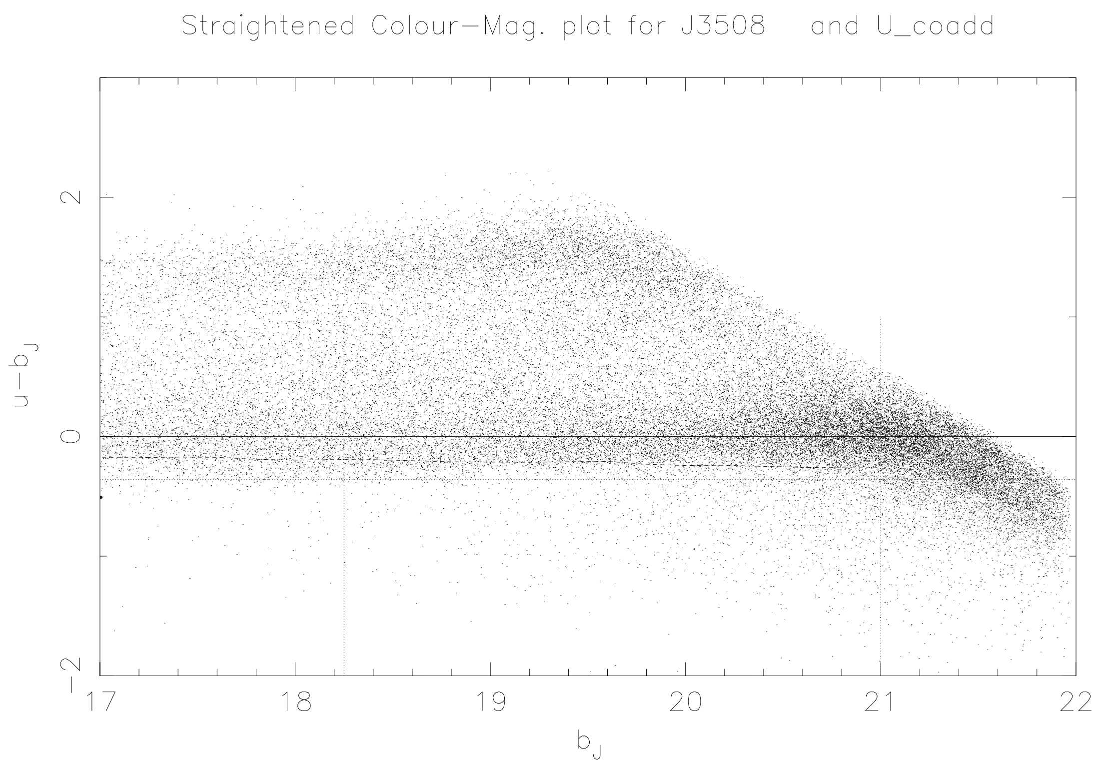

Figure 4.7: Colour-magnitude plots: continued

4.3.1 Photometric errors

Random photometric errors will have a significant effect on the completeness and contamination of the survey at our faintest limits. In order to quantify these we have carried out two tests. The first makes use of the large overlap at 00^{h} RA between f409 and f471. We match all stellar objects with both u and b_{J} magnitudes in this overlap (a total of $\sim$ 4200 images) and calculate the r.m.s. scatter of b_{J}, u and $u-b_{\mathrm{J}}$. Fig 4.11 shows that in the case of these plates the r.m.s. scatter in u and b_{J} are almost identical, $\simeq 0.18$ mag at $b_{\mathrm{J}}=21$. As we move brighter the error on the b_{J} magnitudes drops below the u errors until $b_{\mathrm{J}} \simeq 19.2$. The error in the colour falls quickly from 0.25 at $b_{\mathrm{J}}=21$ to 0.2 only 0.3 mag brighter, tending to ~ 0.1 at the brightest magnitudes. The f409 and f471 fields have u plate limits of $u=$20.8 and 21.4 respectively, so f409 will contribute a larger fraction of this error than f471. However a combination of the two plates should give an approximation to the errors from an average plate in the sample.

The second test is to measure the width of the stellar locus as a function of b_{J}. Fig. 4.12 shows the half-width of the stellar ridge-line, calculated from the peak of the ridge to the $u-b_{\mathrm{J}}$ value corresponding to half the maximum counts. This is only carried out on the blue side of the ridge, removing the effect of the large number of red stars at $u-b_{\mathrm{J}}>0$. We have split the 15 fields into 4 groups, based on the depth of the u plates in each field. As well as plotting the widths for the individual fields

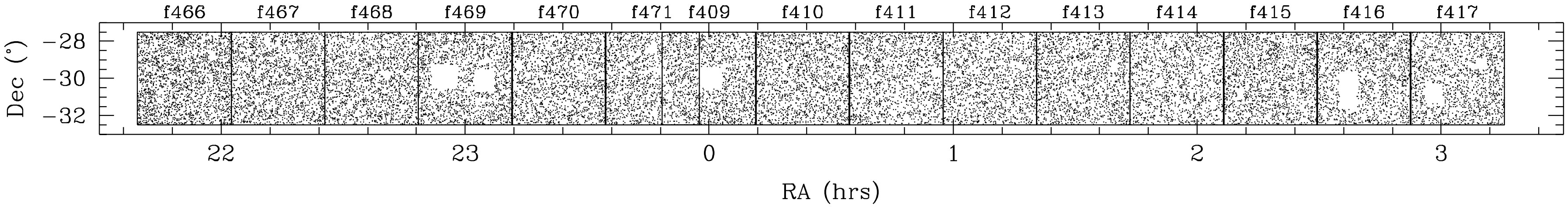

Figure 4.8: The Southern survey region of the 2dF QSO survey. Note the stellar gradient across the strip (due to increased contamination from galactic stars nearer the galactic bulge) and the hole regions cut out of the survey around bright stars.

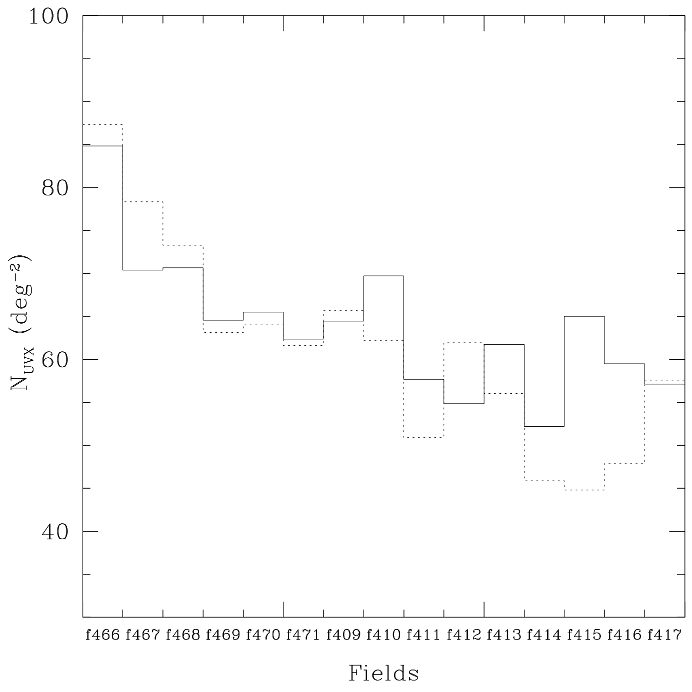

Figure 4.9: Histogram of the number density of UVX objects along the Southern strip, with the fields in order of Right Ascension. The solid line shows the number density of candidates without plate edge matching, while the dotted line includes plate edge matching.

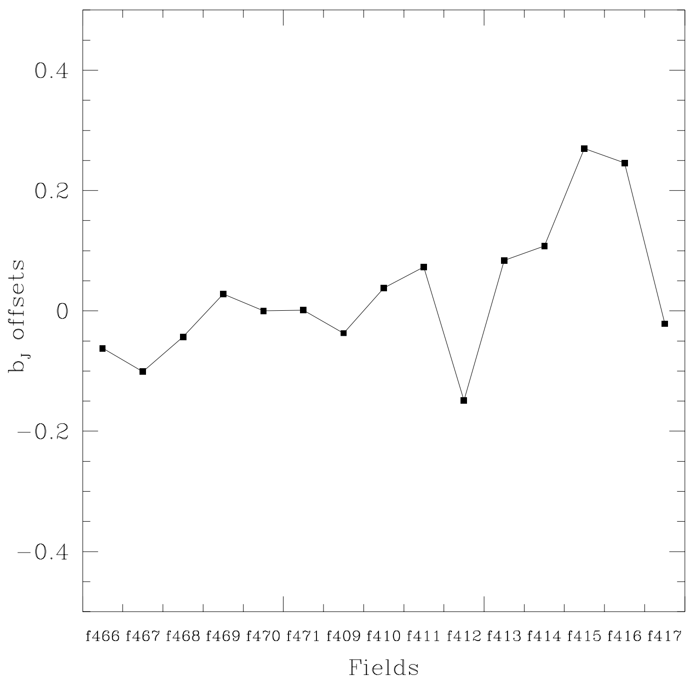

Figure 4.10: Plot of the plate-to-plate zero-point corrections as measured from matching plate-edge overlaps. The fields are in order of Right Ascension. Errors on each measured zero-point offset are $\sim 0.003 - 0.004$.

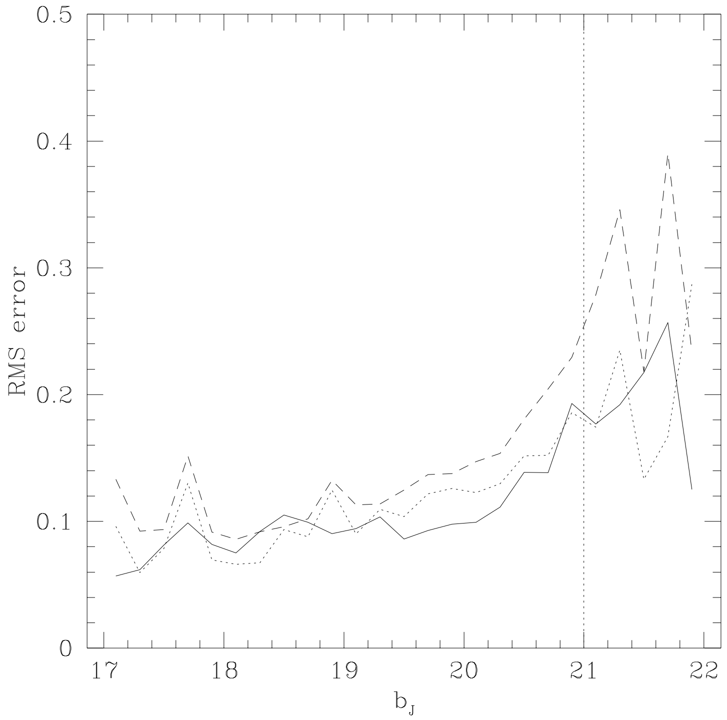

Figure 4.11: The RMS error on b_J (solid line), u (dotted line) and $u - b_J$ (dashed line) as a function of b_J measured from the overlap of the f409 and f471 fields. The vertical dotted line signifies our survey limit of $b_J = 21$.

we have also plotted an average of each of the groups. There are several points of note concerning these diagrams; first, the width at the faint end of the distribution is strongly dependent on the u plate limits, with the shallower plates having widths of ~ 0.4 at $b_J \simeq 21$. For deeper plates this is closer to 0.2. Over the magnitude range $18.5 < b_J < 20$ the ridge-line width is consistently at the $0.16 - 0.18$ level, for all 15 of the fields, suggesting that the photometry over this region is largely independent of the depth of our plates. At brighter magnitudes the smaller numbers of objects increases the noise of the width estimate, however a distinct increase in width is still observable, from ~ 0.18 to 0.25. There are two possible reasons for this increase at brighter magnitudes; either the photometric errors increase, for example due to the effects of increased saturation in the photographic plates, or there is an intrinsic broadening of the locus over this range. The r.m.s. errors from the f409/f471 overlap (Fig. 4.11) suggest that the increased width in the stellar locus is indeed an intrinsic property, and that the errors in both b_J and u tend to ~ 0.1 mag at bright magnitudes.

4.3.2 Measures of completeness from known QSOs

There are more than 200 known QSOs in the Southern strip survey region. These objects have been taken from the Veron-Cetty & Veron (1996) catalogue and have been identified using a variety of techniques. They include UVX, objective-prism,

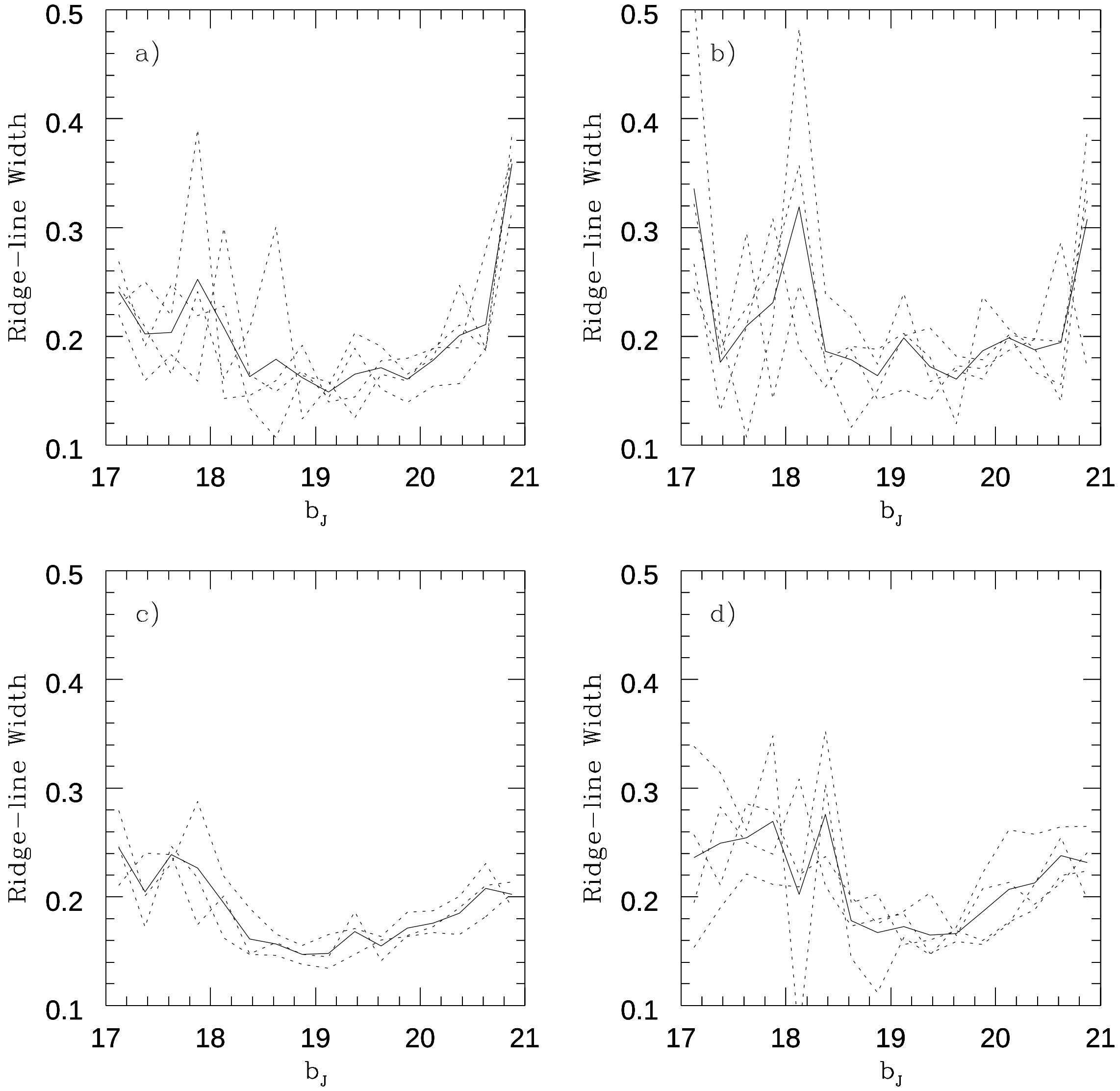

Figure 4.12: The ridge-line half-width as a function of b_J. Fields are grouped according to the limit of the deepest u plate in the field. a) The fields with the shallowest u plates, f409, f410, f413 and f415, $u_{\rm lim} = 20.8 - 20.9$; b) f411, f414, f416 and f412, $u_{\rm lim} = 21.0 - 21.3$; c) f467, f468 and f471, $u_{\rm lim} = 21.4$; d) the fields with the deepest u plates, f466, f417, f469 and f470, $u_{\rm lim} = 21.5 - 21.6$. The dotted lines are for individual fields while the solid lines denote the average of the 3 or 4 fields in each plot.

Table 4.5: Numbers of known QSOs in our survey region

Identification	Number
Total	224
Detected	213
Detected and selected	174
Not detected	11
Non-detections:	
Stellar	1
Galaxies	2
Mergers	8

X-ray and radio selected QSOs. Although the distribution is not homogeneous, the number of these QSOs which we select will tell us whether we are selecting a large fraction of the known QSO population.

We find a total of 224 previously known QSOs within our survey area, over the magnitude range $17.0 < b_J < 21.0$ and the redshift range $0.3 < z < 2.2$. These are matched to the stellar catalogue (both UVX and non-UVX) with a maximum positional difference of $10''$. Details of this are shown in Table 4.5. We find that 11 of the known QSOs are not detected. These 11 comprise 8 objects which were classified as mergers, 2 which were classified as galaxies, and a single stellar object. Each of these was checked by eye using images from the Digitized Sky Survey (STScI), and the mergers and galaxies show nearby, $< 5''$, companions or faint extensions. The object classified as stellar has no matched u magnitude. We are then left with 213 known QSOs for which we have matches in our stellar catalogue. It should be noted that of these, 83 QSOs are UVX selected from the Durham/AAT sample (Boyle et al., 1990).

We take these 213 known QSOs and determine the fraction selected as UVX in our catalogue. Fig. 4.13a shows the number-magnitude relation for these objects. Although this is an inhomogeneous sample, this plot shows that we have significant numbers of QSOs over the range $17.5 < b_J < 21$. Fig. 4.13b shows the colour histogram for the sample. Of the 213 detected QSOs we select 174, that is 82%. Inclusion of the unmatched QSOs reduces this to 78%. Below we try to determine the cause of this incompleteness.

From Fig. 4.13c it is clear that there are several QSOs which are extremely red, 13 QSOs (6%) have $u - b_J \geq 0.0$. In the range $b_J = 19 - 20$ there are a number of QSOs which lie just redward of our original colour selection limit, as well as those already discussed with $u - b_J > 0.0$. In the range $b_J = 20 - 21$ we see that there is a broader spread of QSOs with colours redder than the $u - b_J = -0.36$ limit. This suggests that the incompleteness is at least partially due to photometric errors, although we note from our previous analysis that the photometric errors even

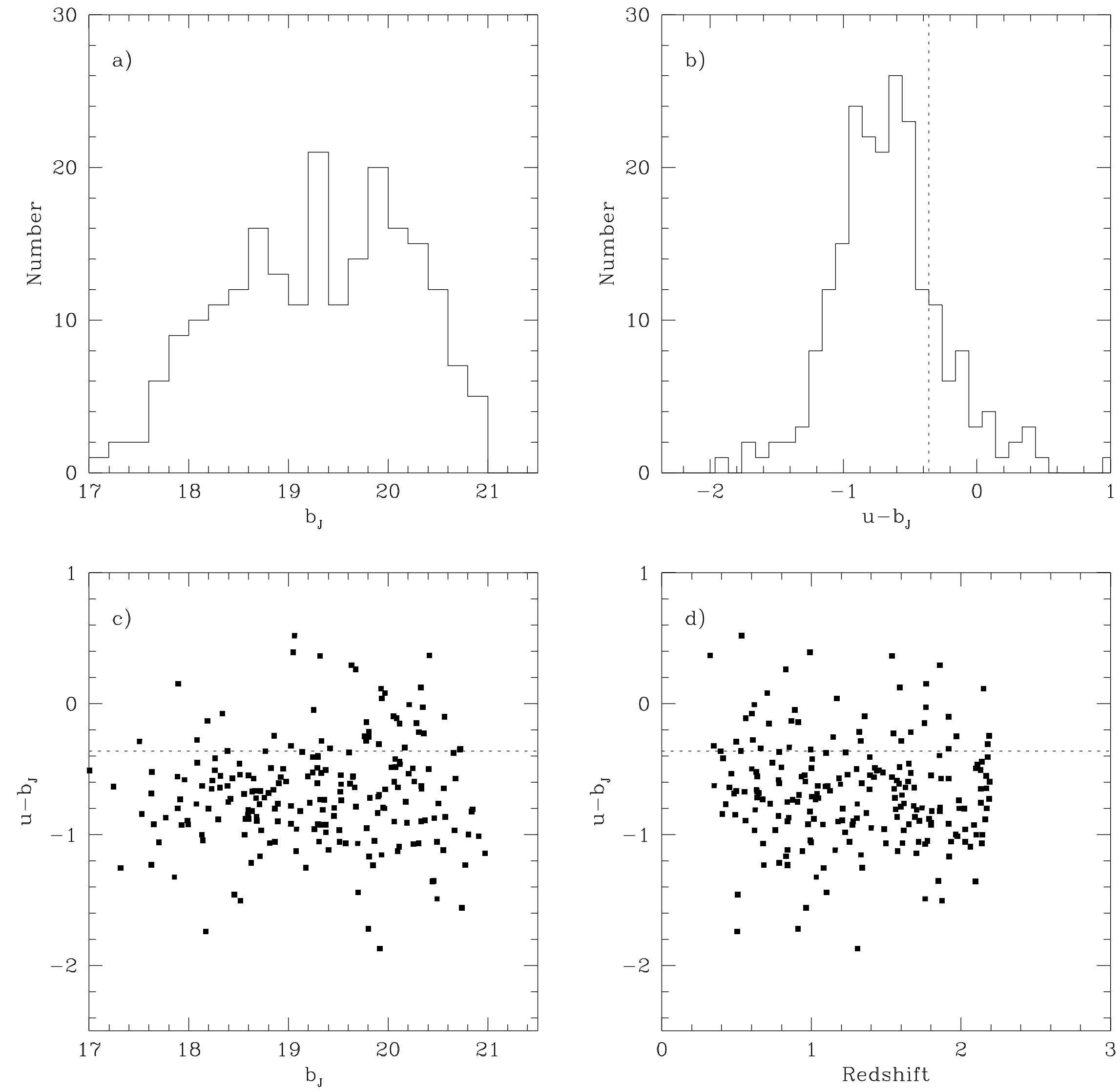

Figure 4.13: The previously known QSOs that have been matched to stellar objects in our survey region. a) the number magnitude relation for this sample, b) a histogram of the colour distribution, c) a colour-magnitude plot, d) a colour-redshift plot. The dotted lines in b), c) and d) show the $u - b_{\rm J} < -0.36$ colour selection criterion.

at $b_J = 21$ are only at the 0.25mag level, or less for fields with deep u plates. The distribution of $u - b_J$ with redshift (Fig. 4.13d) appears to be reasonably uniform, but does not show the tight relation found by Hawkins & Veron (1995).

4.3.3 2dF vs. Durham/AAT

A possible test to ascertain the source of this incompleteness is to compare the 2df UVX catalogue colours of QSOs and stars found in the Durham/AAT sample. The SGP field from this survey overlaps with the f411 field of the current sample. Boyle et al., (1990) use plates J3721 and U6380 to obtain $u' - b$ colours (these magnitudes are defined below) for their QSO candidates (these plates were taken on the dates 4/11/77 and 15/09/80 respectively). In this section we aim to compare the magnitude systems of the two surveys, as well as compare the photometry of the QSOs and stars.

The magnitude system used by Boyle et al., is somewhat different from the one used in the present sample. b is defined as the photographic magnitude zero-pointed to the instrumental CCD magnitude of the photometric calibration sequences. It is related to the standard Johnson B via

$$b = B - 0.28(B - V - 0.9) \tag{4.9}$$

where $(B - V) = 0.9$ is the average colour of the calibrating stars. It should be noted that Boyle et al., (1990) use a different relation, replacing -0.28 with -0.23. Kron (1980) found a relation between photographic b_J and Johnson B which was $b_J = B - 0.23(B - V)$, but this was derived using the GC385 filter to define the b_J band. A preferable transform for the GC395 filter, used for the Durham/AAT and 2df samples, is that derived by Blair & Gilmore (1982), Eq. 4.1. This then gives a conversion from the b system used in the Durham/AAT catalogue to the b_J system used in the present sample,

$$b_J = b - 0.252 \tag{4.10}$$

This relation implies that the 2dF UVX sample, with its limit of $b_J = 21$, is slightly deeper that the Durham/AAT, which had an average limit of $b = 21$. The 2dF sample u magnitudes were derived using stellar locus fitting, while the Durham/AAT u' magnitudes use CCD calibration combined with an extrapolation, assuming a straight stellar locus. The U CCD photometry in the f416 and f466 fields show that locus straightening does indeed produce a linearized magnitude scale. However, there is a average zero-point offset between the 2dF ridge-line magnitudes and the CCD magnitudes of 0.20 mag. In contrast, Georgantopoulos (1991) found an offset between the u' magnitude scale and the standard Johnson U magnitude of -0.2 mag in the SGP field. We have no independent U photometry in the f411 field to confirm the u zero-point, but note that if the same u zero-point offset in f416 and f466 also applied to the f411 field we would expect that the u' and u magnitudes will have a difference of ~ 0.4 mag.

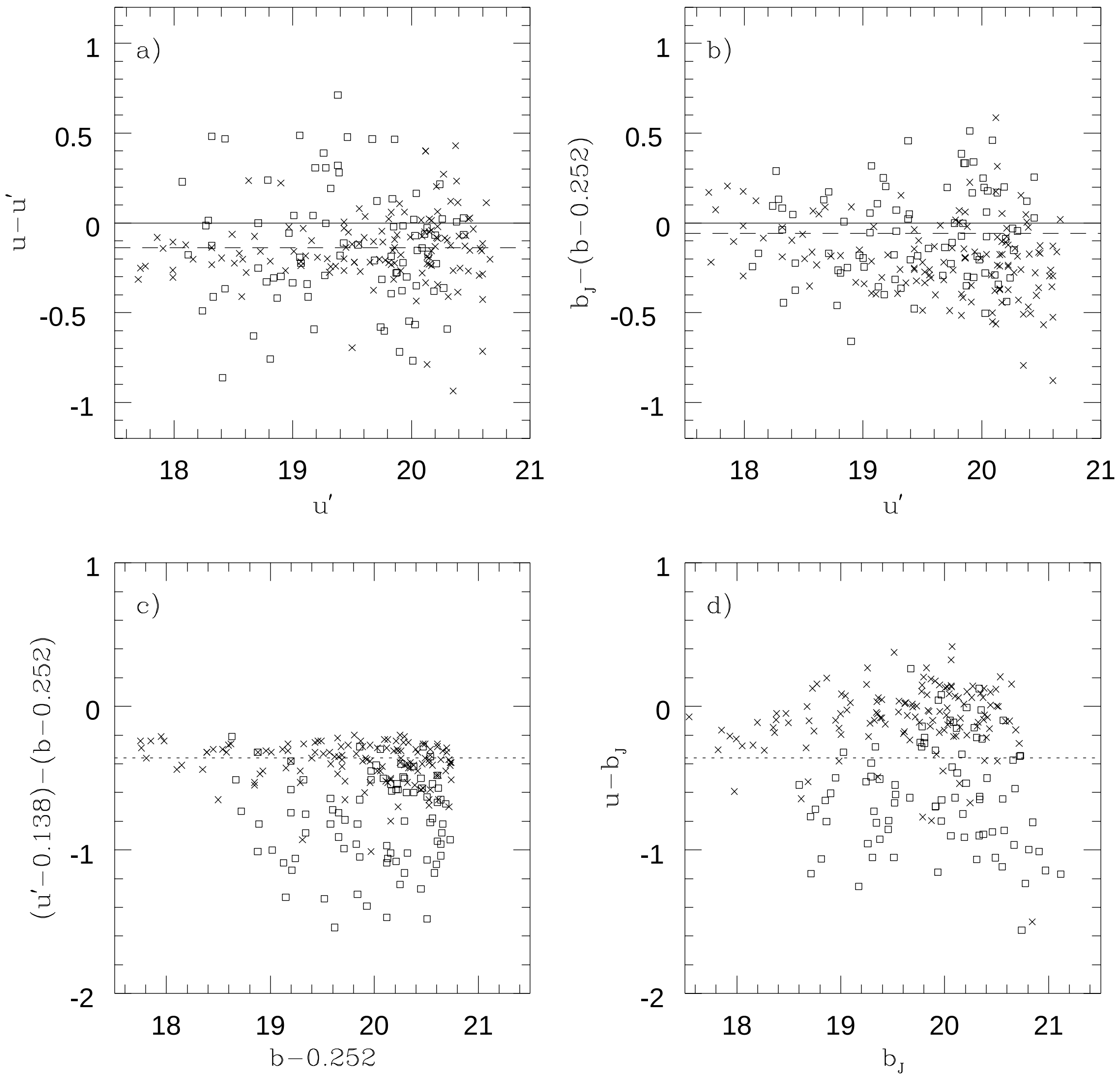

Figure 4.14: A comparison of photometry from the Durham/AAT and 2dF samples for QSOs (open squares) and UVX stars (crosses). a) $u - u'$ as a function of u', the solid line is $u - u' = 0$, the dashed line shows the mean offset for the QSOs. Note that the wider dispersion for QSOs is probably caused by variability. b) $b_J - (b - 0.252)$ as a function of u', the dashed line is the mean offset for QSOs. c) colour-magnitude diagram for the Durham/AAT photometry corrected to the 2dF magnitude system. d) colour-magnitude diagram for the 2dF photometry. Dotted lines in c) and d) show $u - b_J$ cut for the 2dF survey.

Table 4.6: The r.m.s. scatter between Durham/AAT and 2dF magnitudes for stars and QSOs.

	Stars			QSOs		
u	No.	r.m.s. $(u-u')$	r.m.s. $(b_{\rm J}-b)$	No.	r.m.s. $(u-u')$	r.m.s. $(b_{\rm J}-b)$
18–19	26	0.136	0.204	21	0.363	0.249
19–20	48	0.135	0.172	41	0.359	0.259
20–21	56	0.243	0.252	21	0.232	0.254
18–21	130	0.190	0.215	83	0.354	0.291

The plates used for candidate selection in the f411 field are J4606, U15202, U15227 and U15719 (exposure dates, 25/10/78, 1/10/92, 21/10/92 and 20/08/93 respectively). Clearly there is a significant interval between the epochs of the III-aJ and u plates. While the epochs of the III-aJ plates used in the two surveys are similar the epochs of the u plates for the two samples differ by $\sim$ 12 years. Fig. 4.14a shows a comparison of the u-band magnitudes for objects detected by both the Durham/AAT sample and the 2dF QSO survey. While the stellar magnitudes follow a tight relation, which broadens at faint magnitudes (due to increased photometric errors), the QSO distribution has a much larger scatter. The measured r.m.s. scatter for the stars is 0.19 mag, while for the QSOs this is 0.35 mag. When the r.m.s. is calculated as a function of magnitude the difference is even clearer; these data are listed in Table 4.6. Brighter than $u'=20$ the QSO distribution is clearly broader than that of the stars, while in the $u'=20-21$ bin the widths are similar. A similar plot is shown for the $b_{\rm J}-(b-0.252)$ magnitude difference in Fig 4.14b. Here is it clear that the scatter in the QSO distribution is considerably less than for the u-band, while the stellar distribution has more scatter. The r.m.s. scatter in magnitude bins is shown in Table 4.6. The QSO magnitude differences, while still larger than that of the stars, is consistently smaller than the u-band difference measured. This difference between stars and QSOs in the u photometry can most easily be explained as due to variability of the QSOs.

The mean offset between u magnitudes are -0.144 for the stars and -0.129 for the QSOs. There is therefore an average offset of -0.138 between the two sets of photometry, which is somewhat different from the expected -0.4 difference. This possibly suggests that there are other effects which we have not accounted for when comparing the zero-points of the two sets of photometry. The $b_{\rm J}$ and $b-0.252$ magnitudes are offset by -0.198 mag in the case of the stars, but by only -0.060 mag in the QSOs. This will be largely due to the stars being scattered into the selection by photometric errors.

By making an approximate conversion from the old magnitude system to the one used in the 2dF catalogue, we produce Fig. 4.14c which can be compared directly to Fig. 4.14d, containing the new photometry for these objects. It should be noted that a correction to the u' magnitudes has been made which is the average offset of all objects between the u' and u systems. The comparison between the new and old photometry suggests that the colour selection limit for the Durham/AAT sample appears to be, at $u - b_J \simeq -0.2$, somewhat redder than the 2dF survey limit.

4.3.4 A calculation of 2dF survey completeness

Now we compute the expected completeness of our catalogue due to photometric errors, variability and our $u - b_J$ cut. The width of the QSO colour distribution is dependent on a number of effects. The intrinsic width is convolved with effects from variability and photometric errors. If we assume that the excess width in $u - u'$ exhibited by the UVX QSOs is due to variability, then variability adds an r.m.s error of 0.24 mag. We assume an intrinsic width for the QSO colour distribution ($0.3 < z < 2.2$) which is also 0.24 mag, measured from the variability selected sample of Hawkins & Veron (1995). A similar value is given by Veron (1983). We have removed the effect of photometric errors which are ~ 0.1 mag for the variability selected sample (Hawkins, 1986). We then combine this intrinsic width with our estimate for variability and the photometric errors in the $u - b_J$ colour measured from the f409/f471 plate overlap. We generate a random QSO population of 100000 QSOs which has the measured number-magnitude relation (Eq. 3.1 and 3.2) and a Gaussian colour distribution with a mean of -0.68 (the mean colour of the known QSOs in our survey area), and a width defined from the above calculation. Integrating over this population we find that 79.4% of these QSOs are selected with $u - b_J < -0.36$. This is consistent with the expected completeness measured from the known QSOs in the survey area of 78%. Without the variability component this percentage rises to 85.7%, suggesting that we are losing $\simeq 6\%$ of QSOs due to variability. If we also remove photometric errors the percentage completeness rises to 90.6%.

It is therefore clear that with the current UVX colour limit we miss a number of QSOs ($\sim 21\%$). However our main objective was to produce a catalogue which contained a low level of contamination as well as a high number density of QSOs. With this in mind we chose the limit of ~ 62.5 candidates per deg^2 (200 candidates per 2dF field) on average over the survey area. The expected number density of QSOs at our survey limit is 44 per deg^2. Allowing for the $\sim 21\%$ incompleteness, this leaves 35 QSOs per deg^2 and thus we expect over 50% of our candidates to be QSOs. This should be compared to the Durham/AAT sample in which only one third of candidates were successfully identified as QSOs.

4.4 Conclusions

In this Chapter we have discussed the production of a new UVX catalogue to be used as the candidate list for the 2dF QSO survey. We have limited our discussion to the Southern strip; a region of equal area near the North Galactic Cap has also been produced. This will be outlined along with further details of the plate flattening process in Smith (1997). In particular, we have looked in detail at the photometric properties of the catalogue, and carried out several tests to ascertain the levels of completeness expected from the spectroscopic follow-up of the candidate list. We draw the following conclusions:

1) The Southern catalogue consists of 22000 stellar UVX objects covering an effective area of 355 deg^2. Objects were selected from photographic $u - b_J$ colours from UKST plates. We use a process which corrects the photographic plates for field effects. The corrected magnitudes in b_J were calibrated using independent CCD sequences in each UKST field. The u magnitudes were calibrated by defining the position of the galactic star ridge-line to be $u - b_J = 0$.

2) In two fields U-band CCD photometry was available. This shows that the photographic u photometry from ridge-line straightening was linear, although with a possible zero-point offset of ~ 0.2 magnitudes.

3) The catalogue selection limit was chosen to be $u - b_J < -0.36$ over the range $18.25 \leq b_J \leq 21.0$. These limits give the required candidate densities defined by our observational constraints.

4) We measure the r.m.s. and systematic photometric errors present in the catalogue. The r.m.s. errors in colour are ~ 0.15, increasing to ~ 0.25 mag at the very faint end of the catalogue. When we attempt to match the photometry across plate edges we produce a systematic gradient across the survey area. This suggests that there still exist some low level systematic errors at the edges of the photographic plates which have not been removed by our field effect correction process. We do *not* use plate-edge matching to calibrate our catalogue.

5) We estimate the completeness of the survey from the previously known QSOs in our sample. Over the redshift range $0.3 < z < 2.2$ this estimate gives a completeness of 78%.

6) By comparing the 2dF survey photometry of QSOs and stars selected as UVX in the Durham/AAT catalogue, we determine that variability is a significant effect in our catalogue, accounting for $\sim 6\%$ incompleteness. Modelling the contributions from photometric errors, variability and intrinsic scatter we calculate an expected completeness of 79%.

The UVX catalogue with a completeness of $\sim 80\%$ should produce a QSO survey with a high number density, ~ 35 deg^{-2}, allowing us to make effective measurements of large-scale structure on a range of scales. The first spectroscopic observations of this catalogue will allow us to ascertain whether the estimates of completeness discussed here are indeed correct. Discussion of these observations, and a possible way to improve the survey completeness by utilizing UKST r plates can be found in Chapter 6.